

**COMPUTATIONAL METHODS AND MACHINE LEARNING FOR
HIGH-FIDELITY AEROSTRUCTURAL DESIGN OPTIMIZATION**

A Dissertation
Presented to
The Academic Faculty

By

Sean Engelstad

In Partial Fulfillment
of the Requirements for the Degree
Doctor of Philosophy in the
School of Engineering
Department of Aerospace Engineering

Georgia Institute of Technology

March 2025

© Sean Engelstad 2025

COMPUTATIONAL METHODS AND MACHINE LEARNING FOR HIGH-FIDELITY AEROSTRUCTURAL DESIGN OPTIMIZATION

Thesis committee:

Dr. Graeme Kennedy, *advisor*
Department of Aerospace Engineering
Georgia Institute of Technology

Dr. Kai James
Department of Aerospace Engineering
Georgia Institute of Technology

Dr. Christos Athanasiou
Department of Aerospace Engineering
Georgia Institute of Technology

Dr. Vinay Goyal
Department of Aerospace Engineering
University of California Los Angeles

Dr. Elizabeth Qjan
Department of Aerospace Engineering
Georgia Institute of Technology

Date approved: To Be Determined

ACKNOWLEDGMENTS

Thank thesis committee members here.

Thank friends and colleagues.

TABLE OF CONTENTS

Acknowledgments	iii
List of Figures	vi
List of Acronyms	viii
Chapter 1: Introduction and Background	1
1.1 Nonlinear Physics in the Design of Aerospace Vehicles	1
1.1.1 Geometric Nonlinearity	1
1.1.2 Aeroelastic and Aerothermoelastic Coupling	2
1.2 Aerostructural Optimization	2
1.3 Geometric Programming for Structural Design	3
1.4 Machine Learning	4
1.5 Parametric ROMs	5
1.6 Objectives	6
Chapter 2: Log-Scale Methods for Structural Design	7
2.1 Design Curves for Facesheet Debonding of Sandwich Structures	7
2.2 Log-Scale and Affine Transforms for Panel Buckling	9
2.3 Geometric Programming for Structural Design Optimization	12

Chapter 3: Geometric Nonlinear and Aerothermoelastic Physics	15
3.1 Thermo-Mechanical Nonlinear Buckling of Geometrically Imperfect Cylinders	15
3.2 Aerothermoelastic Design Optimization with FUNtoFEM	16
Chapter 4: Machine Learning for Failure Prediction	21
4.1 Machine Learning to Improve Buckling Predictions for Efficient Structural Optimization	21
4.2 Automated Anomaly Identification of Launch Vehicle Propulsion Systems .	24
Chapter 5: High-Fidelity Geometric Nonlinear Aerostructural Optimization . .	26
5.1 Efficient High-Fidelity Analysis	26
5.1.1 Automatic Differentiation	27
5.1.2 GPU Parallel Computing	27
5.1.3 Scalable Linear and Nonlinear Solvers	28
5.1.4 Aerostructural Coupling	29
5.2 Parametric ROMs for Aerostructural Design	29
Chapter 6: Conclusion	31
6.1 Remaining Publications	31
6.2 Final Discussion	31

LIST OF FIGURES

2.1 Diagram of axisymmetric finite element model of an unvented honeycomb core sandwich structure with a facesheet-core debond under pressure and in-plane loads.	7
2.2 Collapsed design curve $a^* = a^*(P^*)$ from affine transformation becomes bilinear in log-scale, with the bilinear fit on the right.	8
2.3 Diagram of a typical stiffened panel geometry with geometric and loading parameters.	9
2.4 Closed-form buckling loads vs the FEA data for unstiffened panels in the thin-walled regime. The mode shapes A1-A3 and S1-S3 are the axial and shear buckling modes predicted by FEA models from the dataset.	10
2.5 (a) Comparison of axial buckling loads for varying number of N_s stiffeners and fixed $\gamma = 3.0$, with a global to local mode transition occurring as ρ_0 decreases. Parts (b) and (c) show the global to local mode transition as γ or EI of the stiffener increases for (b) 1 stiffener and (c) 3 stiffeners.	11
2.6 The fully-stressed method applied to a simply supported plate under transverse loading. The error against the true optimal thickness design is 2.6%.	12
2.7 The FSD compared with KS-aggregate gradient optimization for different ρ_{KS} inputs on the plate. The error against the true mass by FSD is 1.5% with 0.91 mins runtime.	13
3.1 (Left) Cylinder geometric nonlinear buckling analyses from TACS with $r/t = 300$ [C5], (right) NASA SP-8007 nonlinear load-disp curves for cylinders [85].	16
3.2 FUNtoFEM aerothermoelastic coupled forward and adjoint analysis paths. . .	17

3.3	Delta wing design case from [C4] with (a) the aerothermoelastic optimal design, and (b) the supersonic laminar CFD analysis.	19
3.4	Aeroelastic solutions for three wing-shell structures under $M = 0.77, Re = 1e7$ turbulent flow, from the aeroelastic optimization workshop [C1].	19
4.1	Work from [C3, J2] on machine learning buckling loads. (a) A dataset was constructed of high-fidelity finite element buckling analysis with FSDT shell elements, (b) custom log-scale kernel functions for buckling loads were used to train - (c) a GP surrogate model on the buckling data, and (d) the GP model of buckling was included in FEA structural optimization of a subsonic wing and a supersonic delta wing.	21
4.2	Comparison of GPs with squared exponential kernel vs. the novel buckling kernel.	23
4.3	Failure modes in the pull-up maneuver of the aeroelastic benchmark wing [C1], with the smeared closed-form and GP the GP buckling predictions.	23
4.4	(a) Raw sensor data is fed into the ML model, with (c) the m-distance relabeling improving the \mathcal{F}_1 score by 18% from (b) the un-relabeled dataset to (d) the relabeled dataset. (e) A representative ground stage propulsion system from [114].	25
4.5	Confusion matrix across all timesteps of the time-series LSTM classifier in [J3]. A perfect model has ones on the diagonal indicating the truth and predictions match.	25
5.1	Jacobian assembly and cusparse direct LU solve on the GPU for the uCRM.	28

ACRONYMS

- A2D** a code for nearly automatic differentiation 27
- AD** automatic differentiation 27
- BSR** Block Sparse Row 27
- CAD** computer-aided design 16
- CFD** computational fluid dynamics vii, 1, 17–20
- ESP/CAPS** Engineering Sketch Pad / Computational Aircraft Prototype Synthesis 16, 17
- FEA** finite element analysis vi, 4, 7, 10, 17, 18, 22
- FSD** fully-stressed design vi, 4, 12–14
- FSDT** First-order shear deformation theory vii, 9, 21, 22
- FUN3D** Fully Unstructured Navier Stokes 3D 16, 17, 20
- FUNtoFEM** coupled aerostructural analysis tool vi, 15–20, 26, 27, 29
- GEP** geometric programming 13, 14
- GP** gaussian process vii, 21–23
- KDF** knockdown factors 15
- LSTM** Long-Term Short-Term Memory Network vii, 24, 25
- MDAO** multidisciplinary design analysis and optimization 1, 3, 4, 14
- MELD** Method for Extrapolating Linearized Displacements 17, 26, 27, 29
- ML** machine learning vii, 22–25
- NDE** non-destructive evaluation 7
- RANS** Reynolds-Averaged Navier-Stokes equations 17
- TACS** Toolkit for the Analysis of Composites Structures vi, 10, 15–18, 22, 26

CHAPTER 1

INTRODUCTION AND BACKGROUND

1.1 Nonlinear Physics in the Design of Aerospace Vehicles

Due to high computational cost, high-fidelity design tools are still limited by mesh sizes, only consider part of the structure, and limit the scope of the multidisciplinary design analysis and optimization (MDAO) problems. The goal of this work is to use computational methods and machine learning to reduce computational cost of high-fidelity optimizations.

1.1.1 Geometric Nonlinearity

Geometric nonlinearity refers to nonlinearities in a structure due to large displacements, rotations or loading conditions. In recent years, an increasing number of commercial aircraft have used high aspect-ratio wings to increase aerodynamic and fuel efficiency [1]. However, high-aspect ratio wings are more flexible and require the use of more expensive computational tools in their design - namely geometric nonlinear and aeroelastic analysis.

Geometric nonlinear static analyses use iterative strategies for convergence, which can increase the cost of the structural analysis on the order of 10x. For example, Newton's method is used for stable structures [2], while the Riks method is often used for unstable structures [3]. Due to the higher computational cost, many authors have used low-fidelity beam models of aircraft wings to model the geometric nonlinearity, especially when considering the dynamics of flutter [4, 5, 6]. Recent work by Gray and Martins [7] used a Gauss-Seidel ramping strategy [6] to bring down the additional cost of geometric nonlinearity for high-fidelity aeroelastic design to 10-15%. Still, this makes the cost of nonlinear structural analysis a similar order of magnitude to the computational fluid dynamics (CFD).

1.1.2 Aeroelastic and Aerothermoelastic Coupling

In high-speed vehicles, aerodynamic heating can produce high temperatures in the structure and large through-thickness thermal gradients, which make material nonlinearity and aerothermoelastic coupling effects significant [8]. In the past, aerospace engineers have used low-fidelity methods and analytical models to design high-speed vehicles - such as piston theories, linearized potential flow, and Eckert's reference enthalpy method [9]. Comparisons with high-fidelity solutions show significant errors from excluding material property degradation, thermal stresses, aeroelastic washout [C1], and viscous effects [10]. These low-fidelity tools addressed the limited computing power available at the time, but resulted in higher factors of safety and more conservative designs.

High-fidelity design tools reduce physics errors and produce more optimal designs - which may enable new aerospace technologies such as supersonic transport or hypersonic vehicles. This motivates the need for high-fidelity nonlinear coupled physics design tools.

1.2 Aerostructural Optimization

Let $f \in \mathbb{R}$ the objective function, $\mathbf{x} \in \mathbb{R}^M$ the design variables, $\mathbf{u} \in \mathbb{R}^N$ the state variables, g_i for $i = 1, \dots, m$ the optimizer constraints, and $\mathbf{R} \in \mathbb{R}^N$ the nonlinear physics residual. The optimization of an aerospace vehicle is then an NP-hard constrained optimization below with often $m \sim O(10^3)$ constraints, $M \sim O(10^3)$ design variables and $N \sim O(10^5)$ equations.

$$\begin{aligned} & \min_{\mathbf{x}} && f(\mathbf{x}) \\ & \text{s.t.} && g_i(\mathbf{x}, \mathbf{u}) \leq 1 \quad \forall i = 1, \dots, m \\ & && \mathbf{R}(\mathbf{x}, \mathbf{u}) = \mathbf{0} \end{aligned} \tag{1.1}$$

Optimization strategies include gradient-based methods [11] - such as the direct method, the adjoint method, finite difference, and complex-step; and gradient-free methods - such as genetic algorithms. However, with a high number of design variables, the finite-difference,

complex-step [12] and gradient free methods become very expensive. The adjoint method is often used as it scales better with a high number of design variables [13].

In structural optimization, strength constraints and structural design variables are included for each panel [C1, 14], resulting in a high number of constraints and design variables. Constraint aggregation with the Kresselmeier-Steinhaus (KS) function [15] is often used to reduce the number of constraints and the cost of the adjoint method. However, the optimal design can be quite conservative unless a high ρ_{KS} value is used, which increases computational cost [16]. Lambe explored the idea of a matrix-free optimization [17, 18, 19], which uses constraint jacobian-vector products to allow more constraints, however the constraint aggregation strategy was still cheaper for aerostructural optimization.

High fidelity analyses are tractible due to CPU parallel computing and efficient linear solvers. However, they can be expensive in an optimization with $O(10^3)$ design steps - often limiting the scope of the MDAO problem, mesh size, or only considering part of the structure. In this work, GPU parallel computing, reduced order models and new optimization strategies will be considered to further speedup high-fidelity optimizations.

1.3 Geometric Programming for Structural Design

Geometric programming offers large computational speedups for optimization problems whose objectives and constraints can be written as posynomials - that is polynomials with positive inputs and coefficients [20]. Namely, log-scale transformations are used with the AM-GM inequality to convert nonlinear programming to a convex optimization and linear programming [21]. Solution methods are given in [21, 22], which also extend to the signomial case (negative coefficients). Also, rational polynomials, for panel buckling in section 2.2, can be considered with auxillary constraints and variables [23].

While structural finite element analysis constraints are posynomial in the design and state variables, geometric programming does not allow multi-term equality constraints as this breaks convexity, Hoburg [24]. For structural design, geometric programming applications

have been limited to beam closed-form solutions [24, 25] and truss design [26, 27, 28, 29]. Geometric programming is valid for truss design as once the loads are computed - the constraints are monomials of the local structure member thickness.

It turns out there is an important gap in the literature here. Namely, localized forms of structural constraints are not limited to truss structures [30], but also apply to shell and plate structures such as aircraft wings. Indeed, the fully-stressed design (FSD) method [31, 32] sizes the structure efficiently by evaluating in-plane loads through traditional finite element analysis (FEA) and then using scaling laws to determine optimal panel thicknesses. Closed-form solutions of the FSD method for unstiffened plates and shells under axial and transverse loads already exist through a quartic polynomial solution [33]. However, the fully-stressed design method has not been applied to stiffened structures which are critical to aerospace design, likely as the FSD solution is no longer analytic [34]. In section 2.3, I discuss a new approach to use geometric programming to extend the fully-stressed design method to stiffened structures, which can greatly speedup structural sizing. I also discuss extensions of the FSD method to more general MDAO aerostructural optimization.

1.4 Machine Learning

Machine learning technology has revolutionized image recognition, data science, digital twins, language processing and more [35]. Machine learning models can be divided into two main categories (1) artificial neural nets such as deep neural nets, convolutional neural nets, and transformers [36] and (2) statistical machine learning such as gaussian processes, support vector machines and kernel methods [37]. The main applications of machine learning are for supervised learning such as classification and regression, and unsupervised learning such as dimensionality reduction and clustering [36]. Machine learning has the potential to make huge impacts on the aerospace industry; however, the challenge is in identifying which problems will benefit from machine learning, what the inputs and outputs of the model should be, and which model is best-suited for the problem.

For aerospace vehicles, two main applications include (1) surrogate models that approximate failure modes and other quantities after the analysis is complete, and (2) multifidelity methods and reduced-order models that accelerate high-fidelity analysis and optimization. Section 4.1 discusses my work on gaussian process surrogate models to include more accurate panel buckling loads in an efficient high-fidelity optimization. Section 4.2 details a project on LSTMs [38] which can provide realtime anomaly classification of ground stage propulsion systems. My remaining work on ML will focus on its use in ROMs.

Multifidelity methods can speedup high-fidelity optimizations by using gaussian processes to combine high-fidelity and low-fidelity physics through covariance strategies [39, 40]. Thielen found that multifidelity methods can significantly reduce the number of high-fidelity analyses in aerostructural shape optimization [39, 41], but not for structural sizing. In section 2.3, I discuss strategies to speedup structural sizing which is the driving factor in the number of optimization steps, using log-scale and geometric programming. Also, I will explore the use of kernel based methods in parametric ROMs of section 5.2 for steady-state aerostructural optimization, which is discussed in the next subsection.

1.5 Parametric ROMs

High-fidelity physics often possess an underlying low-rank structure, which is the basis of methods like dynamic mode decomposition (DMD) [42], Koopman operators [43, 44], and Proper Orthogonal Decomposition (POD) [45]. In this work, I'm concerned with parametric reduced order models (ROMs) for steady-state aerostructural coupled analysis and optimization. Parametric model reduction includes intrusive strategies such as global POD [46] and manifold interpolation POD [47], as well as non-intrusive strategies such as operator learning [45, 48]. POD reduced bases can be constructed offline or online, with online methods scaling better for high number of design variable [49]. Also, hyper-reduction is a common strategy to reduce assembly time of the full nonlinear residuals [50, 51, 46].

For aerostructural design, Farhat demonstrated coupled aeroelastic ROMs on unsteady turbulent flows over an F-16 [52, 53, 54]. He found that the global POD method does not work well with mach number and angle of attack parameters, and required Grassman manifold interpolation [47]. Parametric aeroelastic ROMs have also been built with operator learning [55] and on linearization of the fluid PDEs [56] for flutter. However, the operator learning strategy uses cubic spline interpolation and may not scale well to high number of design variables in structural sizing. Fluids ROMs may benefit from kernel POD [57, 58] or POD-kriging [59, 60], even with multifidelity methods [61]; however, kernel POD ROMs may struggle with a high number of design variables as well.

In section 5.2, I discuss plans to develop parametric ROMs for steady-state aerostructural optimization with structural, aerodynamic, and shape variables. Different methods for the fluid ROM will be compared such as global POD, grassman manifold POD, operator learning and kernel POD. Also, a reduced basis of the structural variables from section 2.3 may be used to reduce the number of DVs and make some ROM strategies more tractible.

1.6 Objectives

- 1) Can engineers use **log-scale methods** and their near-convexity to speedup preliminary structural design and optimization?
- 2) How can new **machine learning** technologies be used to improve existing engineering design strategies and failure prevention?
- 3) What are the outstanding challenges in achieving efficient multidisciplinary design and optimizations over nonlinear, coupled physics problems such as **geometric nonlinear structures** and **aerothermoelasticity**?
- 4) Can advancements in **GPU computing** and **parametric ROMs** make nonlinear, coupled physics design optimizations more tractible?

CHAPTER 2

LOG-SCALE METHODS FOR STRUCTURAL DESIGN

Log-scale methods can simplify traditional structural design approaches as they convert nonlinear to nearly-linear functions. First, two projects on sandwich structures and panel buckling are discussed, then my future work on geometric programming for structural optimization is detailed with applications to preliminary design.

2.1 Design Curves for Facesheet Debonding of Sandwich Structures

In launch vehicles, non-destructive evaluation (NDE) is used to inspect for facesheet debonds in the unvented honeycomb core rocket fairing structures. The structure is designed so that the critical flaw size for facesheet debonding is detectable by the NDE tool. An approximate energy method for geometric nonlinear, circular plates was given by Timoshenko [62] and used to predict facesheet debonding of unvented honeycomb core sandwich structures by Goyal [63] under pressure loads. My work, Engelstad [C2, J1], extended Goyal's design curve to account for in-plane loads due to the launch vehicle acceleration.

To develop the design curve, I ran over 1000 FEA models in Abaqus [64], using the Virtual Crack Closure Technique to compute the total energy release rate G of the facesheet

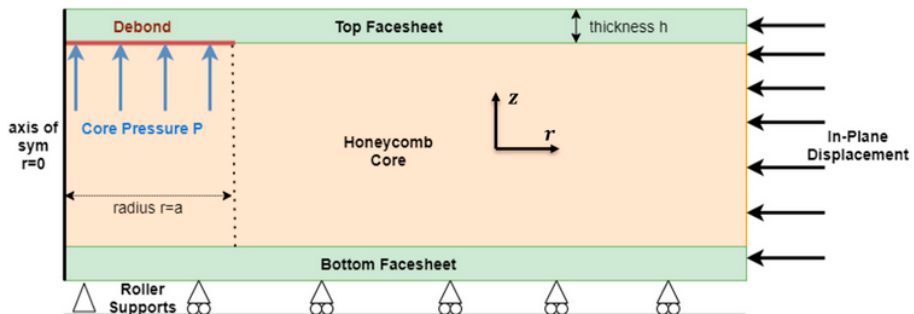


Figure 2.1: Diagram of axisymmetric finite element model of an unvented honeycomb core sandwich structure with a facesheet-core debond under pressure and in-plane loads.

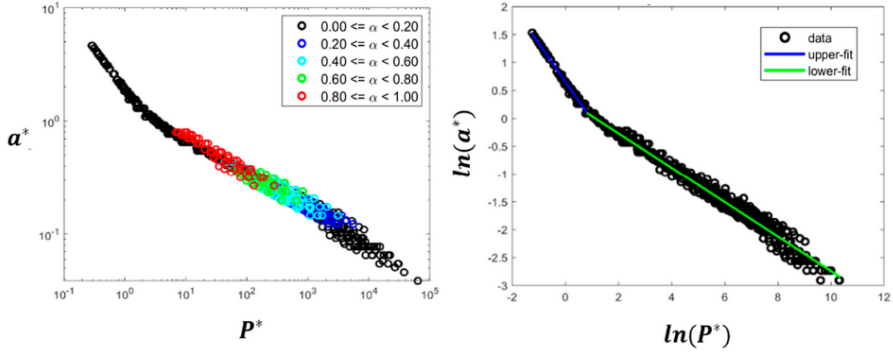


Figure 2.2: Collapsed design curve $a^* = a^*(P^*)$ from affine transformation becomes bilinear in log-scale, with the bilinear fit on the right.

debond. Each model varied a number of parameters including the core pressure P , in-plane strain ϵ , facesheet modulus E , core modulus E_c , facesheet Poisson's ratio ν , facesheet thickness h , and the debond radius a . Figure 2.1 shows a diagram of the axisymmetric finite element models with several of the design parameters included. Two equations, (1) geometric nonlinear equilibrium and (2) the energy release rate equation, were used to solve for the approximate displacement of the center of the debond and the energy release rate G . The two equations were non-dimensionalized; the equilibrium equation is then

$$(1 - \alpha) \cdot \omega_0 + 2\beta\omega_0^3 = \frac{3}{16}a'^4 \quad (2.1)$$

where α is a non-dimensional buckling onset factor, ω_0 is non-dimensional center plate deflection and $a'^4 = (1 - \nu^2)\frac{P}{E} \frac{a^4}{h^4}$ is a non-dimensional flaw size. Also, let $P' = Ph/G$ the non-dimensional energy release rate. The original equations are used to solve the non-dimensional critical flaw size, $a' = a'(\omega_0(P', \alpha))$, resulting in a 2-dimensional surface on (P', α) . An affine transformation (Engelstad [C2]) to the parameters, $P^* = P'|1 - \alpha|^{0.5}\beta^{-0.5}$ and $a^* = a'|1 - \alpha|^{-0.375}\beta^{0.125}$ with $\beta = \beta(\nu)$, collapses to a 1-dimensional curve $a^* = a^*(P^*)$.

Additionally, as the equilibrium equation is polynomial and the energy release rate equation is a rational polynomial, a *log-scale transformation* makes the data *asymptotically linear*. Figure 2.2 shows how a bilinear surrogate model was built in log-space on the

data from the parametric study. The structural engineer then solves the critical flaw size $a = a_c$ with a nonlinear equation solver given the critical energy release rate $G = G_c$ of the material. Also, as many structures closed-form solutions are polynomial or rational polynomial functions, this inspired the use of log-scale transformations in my panel buckling work (section 2.2) and for structural design optimization (section 2.3).

2.2 Log-Scale and Affine Transforms for Panel Buckling

Panel buckling closed-form solutions have been used in preliminary design of aircraft to size for buckling due to their low computational cost. However, the panel buckling closed-form solutions are approximate in that they neglect transverse shear effects [65, 66] or make an infinite aspect ratio assumption in the shear loading case [67]. Recently, improvements to panel buckling closed-form solutions have been extended to First-order shear deformation theory (FSDT) which accounts for transverse shear effects [68, 69], but only for axial loading and certain boundary conditions. Therefore, exact closed-form solutions don't exist for shear loading or intermediate boundary conditions between simply supported and clamped. As panel buckling solutions arise from energy methods [67] like the sandwich structure case, I show here that they also are asymptotic linear in log-scale.

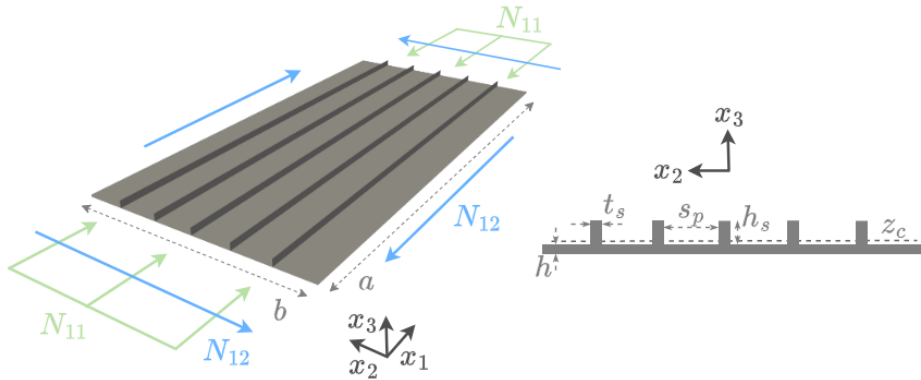


Figure 2.3: Diagram of a typical stiffened panel geometry with geometric and loading parameters.

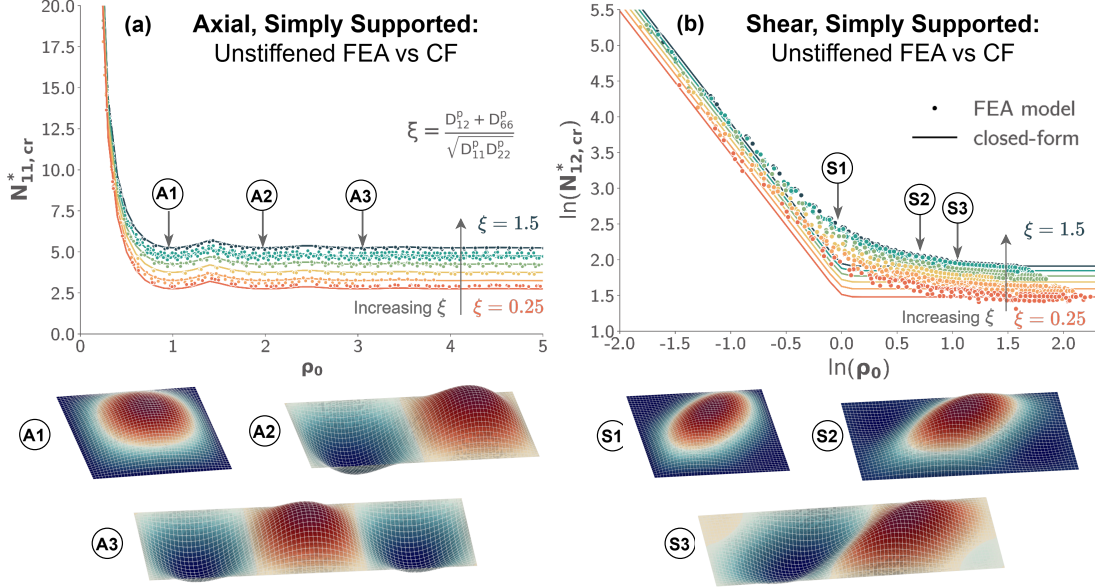


Figure 2.4: Closed-form buckling loads vs the FEA data for unstiffened panels in the thin-walled regime. The mode shapes A1-A3 and S1-S3 are the axial and shear buckling modes predicted by FEA models from the dataset.

Figure 2.3 shows the important parameters in an isogrid stiffened panel design with a the panel length, b the panel width, t_s , h_s the stiffener thickness and height, s_p the stiffener pitch, and N_{ij} the in-plane loads. The global buckling load $N_{11,cr}$ of a stiffened panel under axial loading and simply supported boundary conditions is given by

$$N_{11,cr} = \frac{\sqrt{D_{11}D_{22}}}{b^2(1+\delta)} \cdot N_{11,cr}^*, \quad N_{11,cr}^* = \min_{(m,n) \in N} \left[(1+\gamma) \frac{m^2}{\rho_0^2} + \frac{\rho_0^2 n^4}{m^2} + 2\xi n^2 \right] \quad (2.2)$$

where $N_{11,cr}^*$ is the non-dimensional form of the global axial buckling load, D_{ij} are material [ABD] constants from composite laminate theory [34], $\rho_0 = \frac{a}{b} \sqrt{\frac{D_{22}}{D_{11}}}$ is the affine aspect ratio, $\xi = \frac{D_{12}+2D_{66}}{\sqrt{D_{11}D_{22}}}$ is the laminate isotropy, $\delta = \frac{E_{1s}I_s}{s_p D_{11}}$ is the modulus-area ratio, and $\gamma = \frac{E_{1s}I_s}{s_p D_{11}}$ is the modulus-inertia ratio, with E_{1s} is defined in Ref. [C3]. As the axial buckling load $N_{11,cr}$ is polynomial in the design parameters, it is asymptotically linear in log-scale, with mode switching leading to some additional nonlinearity at intermediate aspect ratios $\rho_0 \sim 1$. Buckling loads from finite element buckling analysis of the Toolkit for the Analysis of Composites Structures (TACS) [70] compared to closed form solutions

are shown for unstiffened panels in Figure 2.4 and stiffened panels with axial loading in Figure 2.5. It is clear that the axial and shear buckling loads are linear asymptotic, with a horizontal asymptote at $\rho_0 \rightarrow \infty$ and a regular linear asymptote at $\rho_0 \rightarrow 0$.

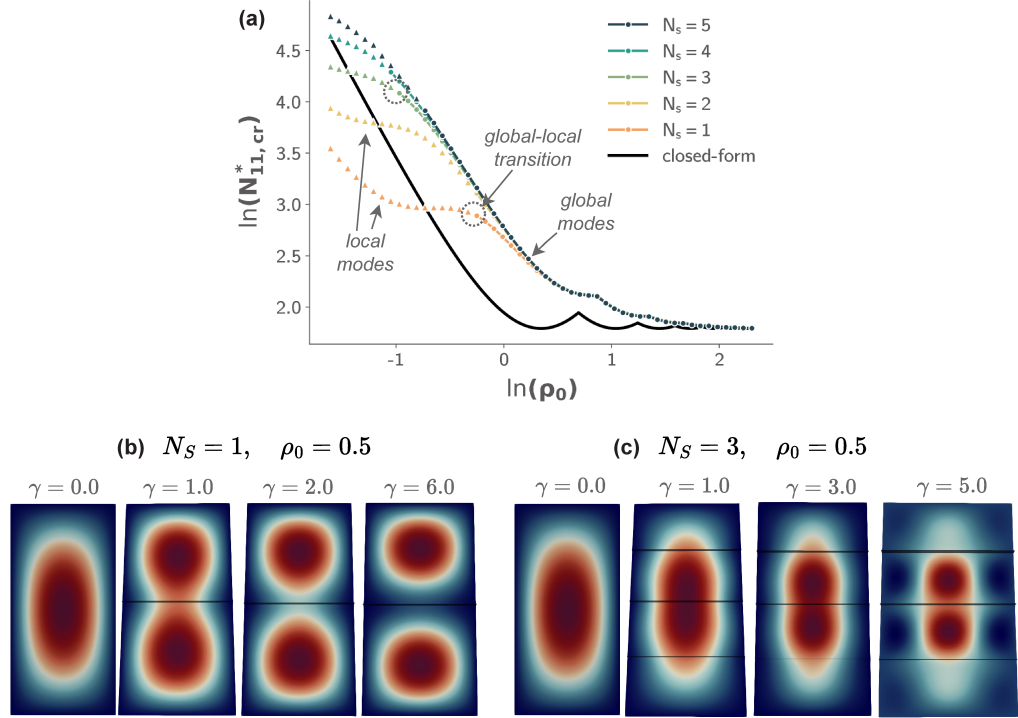


Figure 2.5: (a) Comparison of axial buckling loads for varying number of N_s stiffeners and fixed $\gamma = 3.0$, with a global to local mode transition occurring as ρ_0 decreases. Parts (b) and (c) show the global to local mode transition as γ or EI of the stiffener increases for (b) 1 stiffener and (c) 3 stiffeners.

Figure 2.5 shows a dataset of stiffened panel, finite element buckling analysis, with varying number of stiffeners N_s and stiffener heights h_s . A heuristic, in my work [C3, J2], was used to identify and separate the global and local modes for training machine learning surrogate models of panel buckling in section 4.1. The machine learning surrogate model was trained on the log-scaled parameters which improved model extrapolation.

2.3 Geometric Programming for Structural Design Optimization

In high-fidelity structural optimization literature [14, 71, C4], the minimum weight structural design is achieved by solving an NP-hard nonlinear optimization problem. Constraint aggregation strategies [72, 73, 15] reduce the adjoint cost by lowering the number of constraints. In Kresselmeier-Steinhaus (KS)-aggregation, low ρ_{KS} values reduce computational cost but produce heavier, conservative designs [16]. Thus, accurate aerostructural designs require high ρ_{KS} and computational cost, $O(10^3) - O(10^4)$ CPU-hrs [16, C1]. Here I present a new method that uses geometric programming to speedup structural optimization.

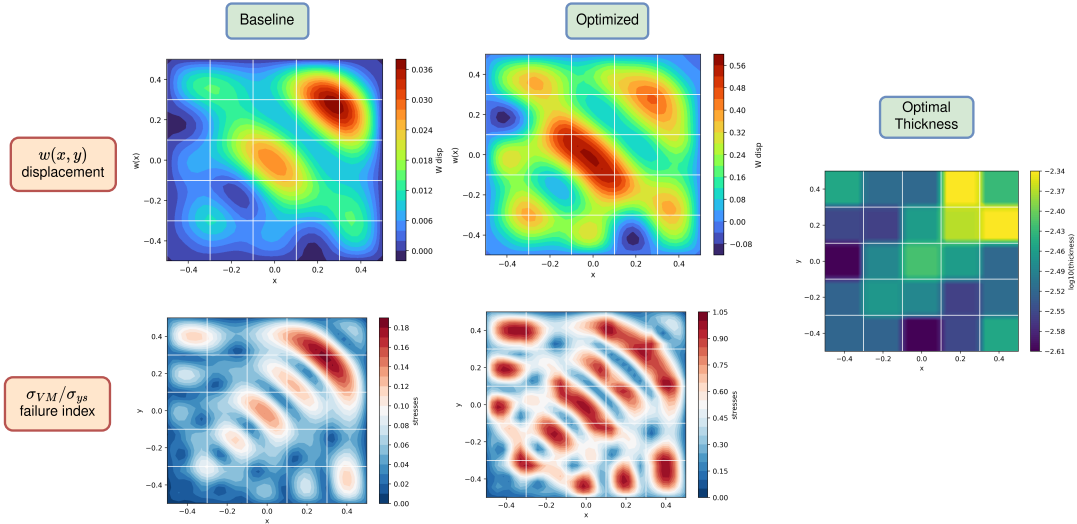


Figure 2.6: The fully-stressed method applied to a simply supported plate under transverse loading. The error against the true optimal thickness design is 2.6%.

An alternative strategy to gradient-based optimization is the stress-ratio method [74, 32, 31, 33], also known as the FSD method [75, 76], for stress-constrained mass minimization. I independently discovered the FSD as the max failure index in each panel was always 1 in our optimal wing designs [C4, C1]. The FSD method assumes the loads in each structural component only depend on local design variables (locality approximation), and the local design variables are updated to drive the failure index to 1. For statically determinate structures, the FSD converges in one iteration while for the general case it converges iteratively.

The FSD method works because the loads in the stress constraint have an auxillary loads PDE, which is nearly design independent. For a transverse plate, the stress σ is proportional to panel thickness h by $\sigma \propto h^{-2}$, so that the FSD design update is $\underline{x}_{k+1} = \underline{x}_k \odot \sqrt{\underline{s}(\underline{x}_k)}$, where the product \odot and square root are element-wise, and \underline{s} are the component max failure indices. The FSD method iterates by (1) computing a forward analysis, (2) computing loads / failure indices in each component, (3) updating the design. Figure 2.6 and Figure 2.7 show the FSD method applied to a plate with 25 thickness design variables, which converged in 6 forward analyses and 0.91 mins runtime. The FSD method achieved an optimal mass 1.5% off the true mass, which is equivalent to the gradient method with $\rho_{KS} \approx 100$, but with a 37x speedup. This demonstrates the usefulness of the FSD method for preliminary design.

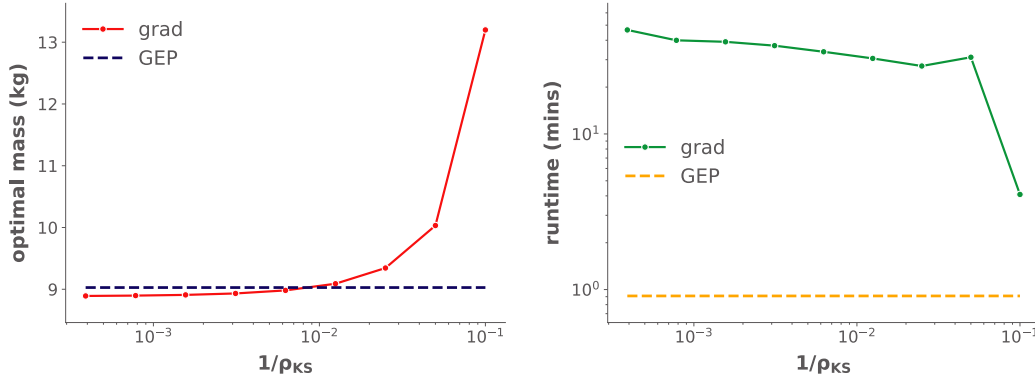


Figure 2.7: The FSD compared with KS-aggregate gradient optimization for different ρ_{KS} inputs on the plate. The error against the true mass by FSD is 1.5% with 0.91 mins runtime.

The FSD method has been applied to plate and shell structures with stress constraints and thickness variables [31, 74] using Newton iteration [31] or quartic polynomial solutions for design updates [33]. For practical aerospace structures, stiffener design variables and global, local panel buckling constraints need to be included [34, 14, J2], which are challenging for traditional FSD. As the stress and panel buckling constraints are polynomial or rational polynomials from section 2.2, they can be approximated by posynomials [24, 25]. Thus, the local optimizations of the FSD method for stiffened structures with 4-5 constraints and 4 design variables in each panel can also be done with geometric programming (GEP) [77, 78].

The approach that I'd like to highlight uses the FSD method with geometric programming for rapid preliminary design structural sizing. Formulating each local optimization problem in FSD with geometric programming allows us to take advantage of log-convexity and convert to a near-linear programming problem. The following steps will be involved in its development, and I intend to apply this to plate and wing design cases.

- The FSD method and geometric programming will be used to perform rapid preliminary design for stiffened aircraft structures.
 - Use Sherman-Morrison-Woodbury matrix inversion [79] to invert A , D matrices with stiffener smearing [34, C3] - to get stresses and strains from the in-plane loads and bending moments for FSD (see [33] for unstiffened closed-form).
 - Use auxillary variables and constraints [80] or posynomial approximations [24, 25] to handle rational polynomial constraints.
 - Solve the local geometric programming optimizations using convex optimization [22] of each element in the mesh on the GPU and take max design updates.
- For tougher MDAO optimizations, try the following:
 - Use GEP-FSD method as initial designs for optimization.
 - Build reduced basis of log DVs from snapshots of GEP-FSD method for MDAO optimization. Use Qjan's reduced basis error bounds [49].
 - I have a proof on inertial load case that log-scaling allows reduced basis method with one or two modes to work, while linear scaling will require many modes.

CHAPTER 3

GEOMETRIC NONLINEAR AND AEROTHERMOELASTIC PHYSICS

At high-speeds and for high-aspect ratio wings, the design of aerospace structures are increasingly driven by nonlinear physics including geometric nonlinear structures [81, 2] and aerothermoelasticity. The following are my preliminary work for high-fidelity analysis and optimization of nonlinear, coupled physics problems. First, a project on thermo-mechanical nonlinear buckling of cylinders illustrates geometric nonlinearity and the challenges of nonlinear structural analysis. Then, a framework for aerothermoelastic coupled analysis and optimization in coupled aerostructural analysis tool (FUNtoFEM) is presented, with some of the current challenges discussed.

3.1 Thermo-Mechanical Nonlinear Buckling of Geometrically Imperfect Cylinders

Geometric nonlinearity and thermo-structural physics are important in the stability of cylindrical rocket fairing structures, which are exposed to mechanical inertial and heat flux loads in hypersonic flight. Also, cylinders are highly sensitive to geometric imperfections [82, 83, 84] (while panels and beams are not), so nonlinear buckling analyses are required to compute imperfection knockdown factors (KDF) for stability. The NASA SP-8007 document [85] gives industry guidelines for KDFs of cylinders under mechanical loadings.

To determine whether these geometric imperfection KDFs on mechanical loads are sufficient for heat flux load cases, I computed KDFs for cylinders with heat flux loads and ring stiffeners using nonlinear buckling analysis in TACS [70], among several different r/t and stiffener designs [C5]. I found that the heat flux loads introduce small biaxial effects near the ring stiffeners which contributes to lower overall buckling loads, but less severe KDFs than the pure mechanical load case due to more benign mode shapes as in Figure 3.1.

Also, log-scale transformations from chapter 2 could be used for cylinders [86, 87, C5]

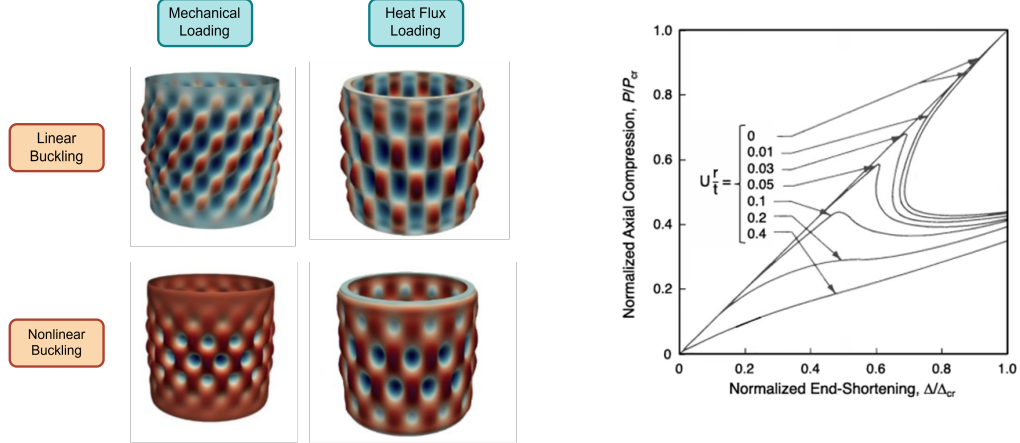


Figure 3.1: (Left) Cylinder geometric nonlinear buckling analyses from TACS with $r/t = 300$ [C5], (right) NASA SP-8007 nonlinear load-disp curves for cylinders [85].

like panel buckling, but it would be more expensive to obtain accurate nonlinear buckling results required for cylinders and there would be imperfection inputs required as well. Also, for section 5.1, the geometric nonlinear static analysis of cylinders required about 10x the solve time of a linear static analysis, with slower convergence at instabilities.

3.2 Aerothermoelastic Design Optimization with FUNtoFEM

A preliminary framework for adjoint-based, high-fidelity aeroelastic optimization with FUNtoFEM was developed by Jacobson and Kiviah [88, 89, 90]. The framework was extended to aerothermoelastic optimization and demonstrated on supersonic panels by Smith [91] and Halim [92]. Brian Burke and I extended the FUNtoFEM framework to aerothermoelasticity with turbulent flows and fixed the adjoint derivative accuracy against complex-step. Also, we've incorporated the parametric CAD tool ESP/CAPS [93, 94], which has been used in aeroelastic shape optimization by Novotny and Sandler [95, 96].

The FUNtoFEM tool uses the nonlinear block Gauss-Seidel method to converge the coupled analysis among separate fluid and structures discipline solvers. Our previous work on the design of supersonic wing [C4] and a subsonic benchmark wing [C1] with FUNtoFEM used the Fully Unstructured Navier Stokes 3D (FUN3D) fluids solver [97, 98] and

the TACS structures solver [70]. FUN3D is a Reynolds-Averaged Navier-Stokes equations (RANS) CFD-solver for unstructured grids with a discrete adjoint [99] and an elasticity-based mesh deformation procedure [100]. TACS [70] is a finite element analysis tool with CPU-parallel computing and an adjoint for structural optimization. ESP/CAPS is used to generate the FEA and CFD discipline meshes [101] for TACS and FUN3D, including mesh sensitivities for shape optimization [102]. Load and displacement transfer is performed by Method for Extrapolating Linearized Displacements (MELD) [103], which transfers aeroelastic states between the fluids and structures meshes. An extension of MELD for aerothermal coupling called MELD-Thermal is also used to transfer temperatures and heat fluxes across the discipline meshes. Finally, the aitken acceleration strategy [104] is used to improve the stability of the coupled analysis algorithm.

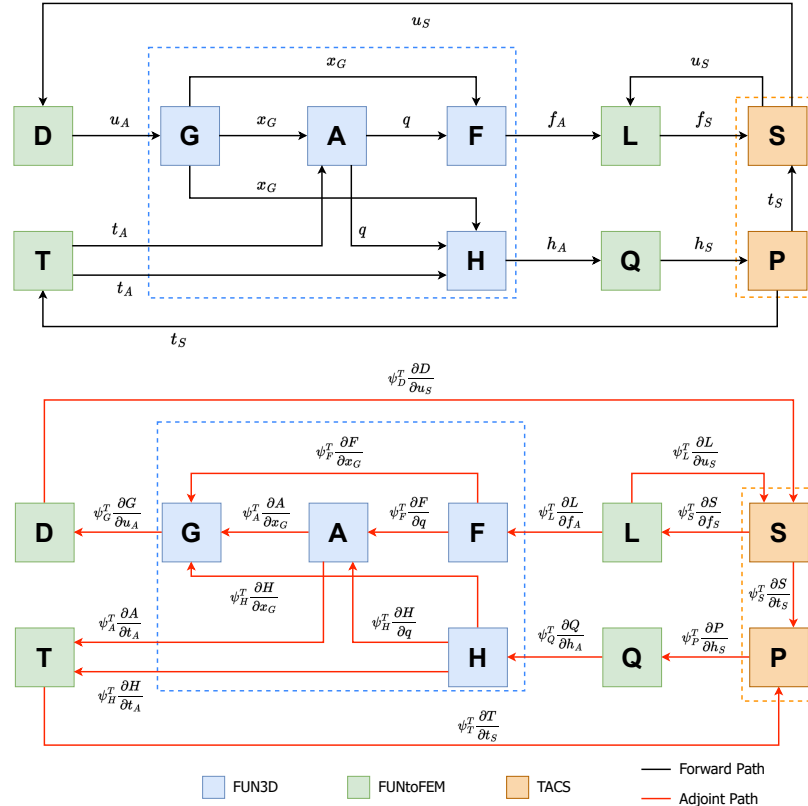


Figure 3.2: FUNtoFEM aerothermoelastic coupled forward and adjoint analysis paths.

The steps involved in the coupled forward and adjoint analysis in FUNtoFEM are

shown in Figure 3.2. The forward analysis state variables are u_S, u_A the structural and aerodynamic displacements; x_G the deformed CFD mesh coordinates; q the aerodynamic or flow states; f_A, f_S the aerodynamic and structural loads; t_A, t_S the aerodynamic and structural temperatures; and h_A, h_S the aerodynamic and structural heat fluxes. The components in the coupled forward analysis and their residuals A, S, P , etc. are the following: L, D the aeroelastic load and displacement transfers; T, Q the aerothermal temperature and heat flux transfers; G the CFD mesh deformation; A the CFD aerodynamic analysis; F, H the CFD boundary computations of force and heat fluxes; and S, P the FEA elastic and thermal structure solves. In our aerothermoelastic design of a supersonic wing, the elastic and thermal structures solves S and P were combined into one linear, thermo-structural analysis in TACS. The residuals for the linear thermo-structural TACS analysis and the CFD analysis are shown below in Equations (3.1) and (3.2). The coupled adjoint equations [92] satisfy the Karush-Kuhn-Tucker conditions, which results in a blocks-sparse linear system on the adjoint variables ψ_A, ψ_S , etc. The coupled adjoint equations are solved through a block Gauss-Seidel coupled analysis that stores adjoint-jacobian vector products, e.g. $\bar{A} = \psi_A^T \frac{\partial A}{\partial x_G}$.

$$S(u_s, t_s, f_s, h_s) = \begin{bmatrix} Ku_S + L_H(t_s - t_{ref}) - f_s \\ K_H(t_s - t_{ref}) - h_S \end{bmatrix} = 0 \quad (3.1)$$

$$A(q, x_G, t_A) = K_A(q; x_G, t_A) \cdot (q - q_0) - r_A(q_0; x_G, t_A) = 0 \quad (3.2)$$

In our first paper on FUNtoFEM [C4], we applied our tool to the design of a hot duct and a supersonic wing. The supersonic wing in Figure 3.3 was designed from a single-point $M = 2, Re = 10^6$ laminar CFD analysis with aerothermoelastic coupling. The wing structure was designed by optimizing panel thicknesses in the outer mold line and internal structure of the wing, with the Kresselmeier-Steinhaus (KS) function used to enforce a stress failure index constraint [16]. Also the SNOPT quasi-Newton optimizer in pyOptSparse [105]. We also used FUNtoFEM in the aeroelastic optimization workshop

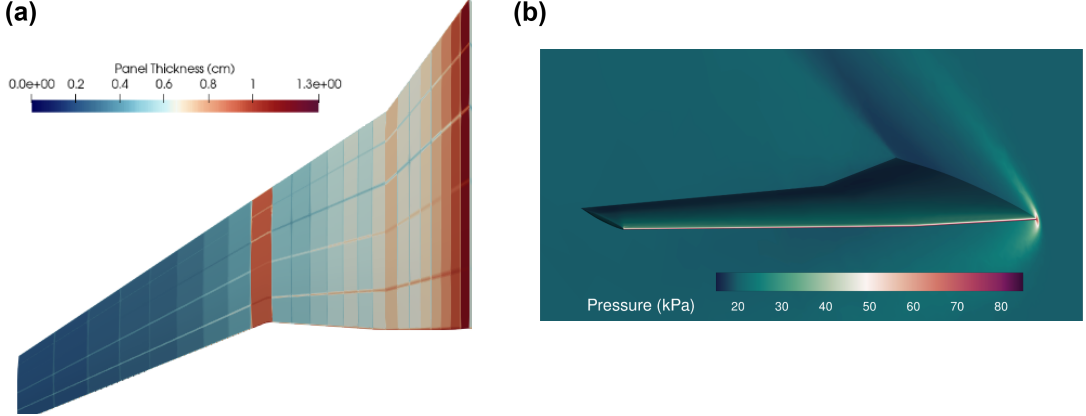


Figure 3.3: Delta wing design case from [C4] with (a) the aerothermoelastic optimal design, and (b) the supersonic laminar CFD analysis.

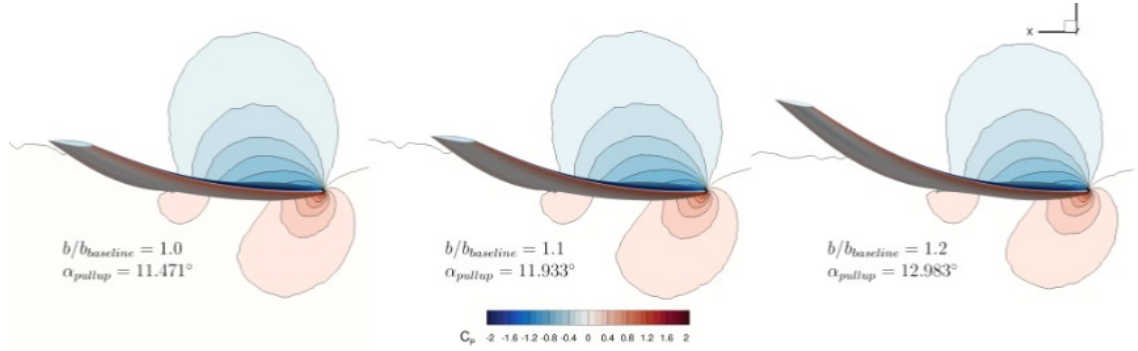


Figure 3.4: Aeroelastic solutions for three wing-shell structures under $M = 0.77, Re = 1e7$ turbulent flow, from the aeroelastic optimization workshop [C1].

[C1] for the design of a subsonic benchmark wing proposed by Gray and Martins[14]. The aeroelastic analysis for three different wingspans of the benchmark are shown in Figure 3.4.

Aerostructural optimization problems are computationally expensive and are primarily limited by the cost of the CFD analysis and the complexity of the optimization problem. In the aeroelastic optimization workshop, we were only able to complete the first of the three benchmark optimization problems due to the high computational cost of our current aerostructural optimization toolset in FUNtoFEM. For example, the forward and adjoint coupled analysis in the case I benchmark problem took about 30 minutes per design on 48 CPU processes. The current challenges in our aerostructural optimization framework include the following:

- The computational cost of the coupled analysis at a single design point, which is driven by the CFD analysis and CFD grid deformation.
- Robustness and convergence speed of the turbulent CFD forward and adjoint problems can be reduced due to aeroelastic coupling effects in our simultaneous convergence strategy (block Gauss-Seidel) for the fluid and structural disciplines in FUNtoFEM.
- Our current structural optimization approach with constraint aggregation makes slow optimization progress on structural design variables, with the optimizer focusing on one or two panels at a time during the first $\approx 50\%$ of the optimization.
- The robustness of the elasticity-based, CFD mesh deformation procedure with turbulent flows in FUN3D, which can fail with negative cell volumes at intermediate designs in the optimization.
 - The negative cell volume failures often occur at structural designs with one or more panels having unreasonably low panel thicknesses.
 - In our current structural optimization approach with constraint aggregation, the gradient has disparate orders of magnitude in the early phases of the optimization, leading to poor optimization conditioning.
 - While we can perform one-way coupled optimizations to improve the initial condition of the full aerostuctural optimization, in shape optimizations these low panel thicknesses at intermediate designs still occur.

Of my completed work, there are still a number of open problems and room for improvement in our aerostructural optimization toolset. For this reason, the majority of my remaining work is going to be focused on solving these problems.

CHAPTER 4

MACHINE LEARNING FOR FAILURE PREDICTION

4.1 Machine Learning to Improve Buckling Predictions for Efficient Structural Optimization

Panel buckling closed-form solutions have been used in preliminary design of aircraft to size for buckling due to their low computational cost. However, the panel buckling closed-form solutions are approximate in that they neglect transverse shear effects [65, 66] or assume infinite or zero aspect ratios in the shear loading case [67]. While linear buckling analyses can be included in a wingbox optimization [106], they can be unconservative to the true nonlinear buckling loads, which are expensive to include in an optimization. Therefore, a gaussian process (GP) [37] surrogate model was built to improve panel buckling predictions, while maintaining a computationally efficient structural optimization [C3, J2].

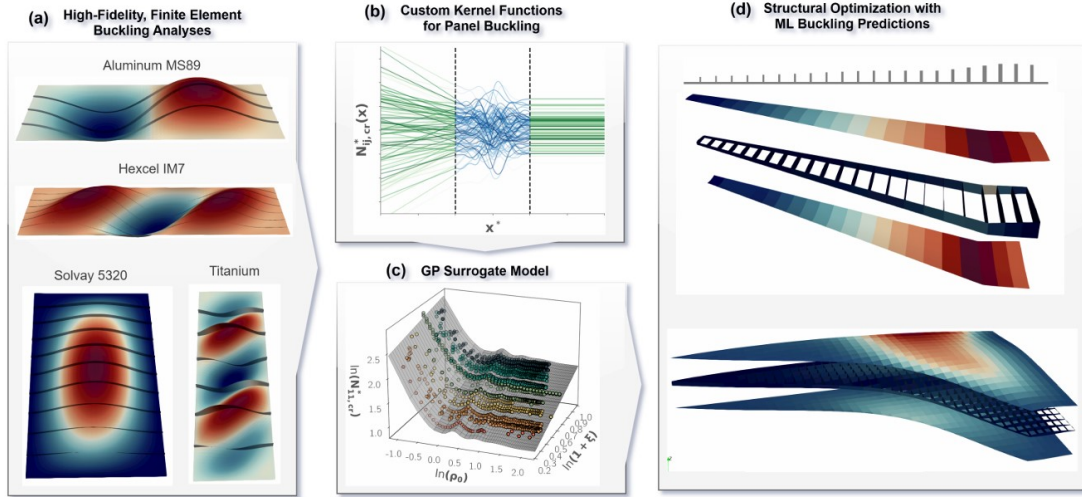


Figure 4.1: Work from [C3, J2] on machine learning buckling loads. (a) A dataset was constructed of high-fidelity finite element buckling analysis with FSDT shell elements, (b) custom log-scale kernel functions for buckling loads were used to train - (c) a GP surrogate model on the buckling data, and (d) the GP model of buckling was included in FEA structural optimization of a subsonic wing and a supersonic delta wing.

Figure 4.1 shows the main steps of training the GP surrogate model from data and then including it in a structural optimization. The finite element buckling analysis training data was obtained from TACS [70] on FSDT shell elements. Custom kernel functions were developed with asymptotic linearity to take advantage of the log-scale transformation discussed in section 2.2. Once the kernel function $k(x, x')$ is chosen, the GP surrogate model is trained on the dataset $X = [x_1, \dots, x_N]$ and $Y = [y_1, \dots, y_N]$ divided into training and testing splits, with each $x = [\ln(\rho_0), \ln(1 + \xi), \ln(1 + \gamma), \ln(1 + 10^3 \zeta)]$ and $y = \ln(N_{ij,cr}^*)$ either the axial or shear buckling loads from section 2.2. Equation 4.1 shows the joint normal distribution for the zero-mean GP with $[\Sigma(X, X')]_{ij} = k(x_i, x'_j)$, and Equation 4.2 shows the test set conditional mean given the training set.

$$\begin{bmatrix} Y_{\text{train}} \\ Y_{\text{test}} \end{bmatrix} \sim \mathbb{N} \left(\mathbf{0}, \begin{bmatrix} \Sigma(X_{\text{train}}, X_{\text{train}}) + \sigma_n^2 I, & \Sigma(X_{\text{train}}, X_{\text{test}}) \\ \Sigma(X_{\text{test}}, X_{\text{train}}), & \Sigma(X_{\text{test}}, X_{\text{test}}) \end{bmatrix} \right). \quad (4.1)$$

$$\mu(Y_{\text{test}}) = \Sigma(X_{\text{test}}, X_{\text{train}}) [\Sigma(X_{\text{train}}, X_{\text{train}}) + \sigma_n^2 I]^{-1} Y_{\text{train}} \quad (4.2)$$

For computational efficiency, the training weights $\underline{\alpha} = [\Sigma(X_{\text{train}}, X_{\text{train}}) + \sigma_n^2 I]^{-1} Y_{\text{train}}$ are saved offline, so that the GP model can be used online with a simple dot product of $\mu(Y_{\text{test}}) = \Sigma(X_{\text{test}}, X_{\text{train}}) \cdot \underline{\alpha}$. Figure 4.2 shows GPs with the standard squared exponential kernel compared vs. the novel buckling kernel, with greatly improved model extrapolation to low and high aspect ratios. Thus, the novel buckling kernels were useful as a wide range of panel designs are considered in the wing optimization cases, and it's difficult to obtain some high γ datapoints as in Figure 2.5 they require a high number of stiffeners. Finally, the GP surrogate model was included in TACS, the FEA tool, with 46% less optimization runtime using the GP buckling predictions in the optimization instead of the closed-form solutions [C3, J2] due to the machine learning (ML) model smoothing out mode switching.

In general, transverse shear effects contribute to heavier ML designs while stronger stiffeners contribute to lighter ML designs with more exact buckling loads. Thus, local

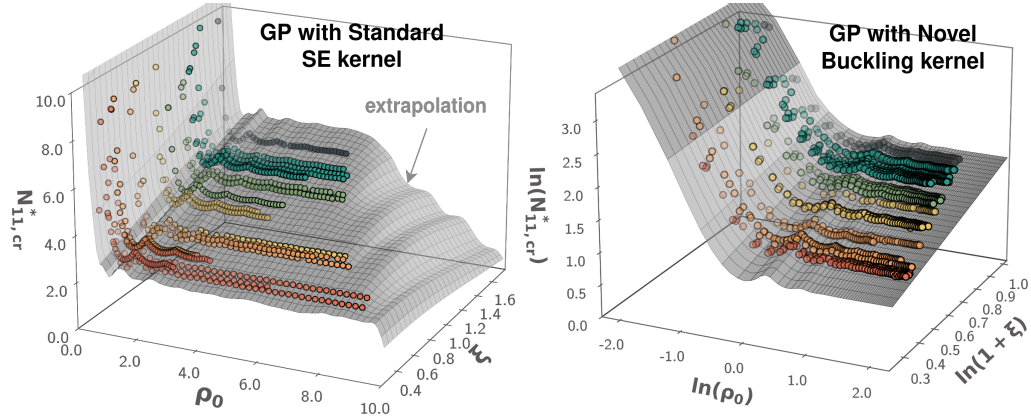


Figure 4.2: Comparison of GPs with squared exponential kernel vs. the novel buckling kernel.

buckling regions (unstiffened) will contribute to lighter ML design while global buckling has a tradeoff, with heavier ML designs only for large stiffeners. This resulted in slightly heavier ML designs of subsonic wings by 0.5% in [J2] and by 6% in the aeroelastic workshop [C1], due to mostly the tip of the wing sized by buckling. In the high-speed civil transport wing wing of [C5], the wing was sized by global buckling quite a bit and the ML design was lighter. The results show that ML buckling models can be used to improve buckling predictions while maintaining computational efficiency in an optimization.

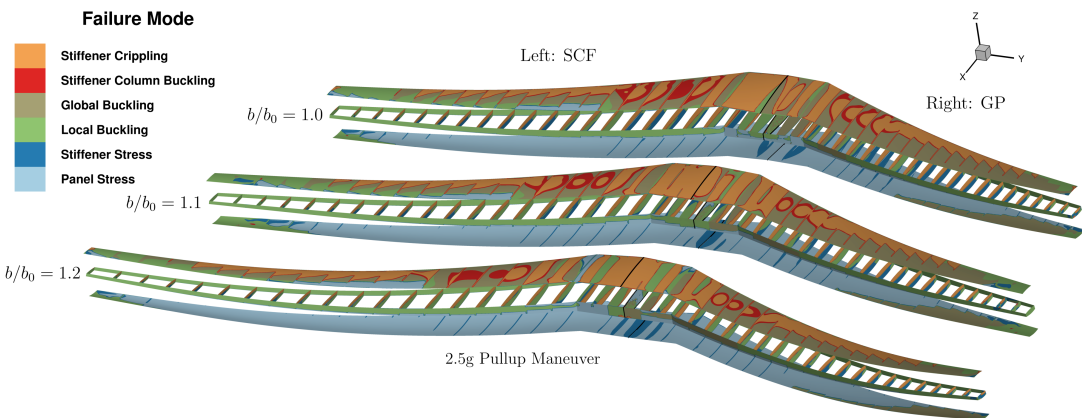


Figure 4.3: Failure modes in the pull-up maneuver of the aeroelastic benchmark wing [C1], with the smeared closed-form and GP the GP buckling predictions.

4.2 Automated Anomaly Identification of Launch Vehicle Propulsion Systems

Launch statistic studies have shown that a large portion of launch vehicle failures are attributed to fluid or propulsion systems [107, 108, 109], with a large portion happening early in a launch vehicle program. With the advent of reusable launch vehicles, the launch industry needs new tools to identify and mitigate propulsion system failures. Our proposed solution is to use machine learning methods for automated anomaly identification.

In the work [C6, J3], the goal was to train a Long-Term Short-Term Memory Network (LSTM) [38, 110], time-series classification model to detect propulsion system anomalies. Monte Carlo simulations of various failure modes of the system were performed by our tool *oldyeller*, with the engine simulations performed by *GiNA* [111]. The machine learning (ML) model was trained to predict the failure probabilities from input sensor data.

The ML model is built in tensorflow [112] with multiple LSTM and EinsumDense layers. Let Y_{ijk} be the truth classification labels for i the trial index, j the time index, and k the class index. The ML model trains a surrogate classifier \mathcal{M} , on the data X and hyperparameters θ , such that the predictions $\hat{Y} = \mathcal{M}(X, \theta)$ minimize the loss \mathcal{L} in Equation 4.3. The confusion matrix C_{mn} and F1 score \mathcal{F}_1 [113] metrics are computed on the test data, with $\delta(\cdot, \cdot)$ the kronecker delta and N_c the number of classes. An \mathcal{F}_1 score of 96.7% was achieved in [J3] with 15,000 trials, 10 seconds of real-time simulation and 20 failure modes, see Figure 4.5.

$$\begin{aligned}\mathcal{L}(Y, \hat{Y}) &= \frac{\sum_{i,j,k} -Y_{ijk} \log(\hat{Y}_{ijk})}{\sum_{i,j} (1)} \\ C_{mn}(Y, \hat{Y}) &= \sum_{i,j} Y_{ijm} \cdot \delta(n, \text{argmax}_k \{\hat{Y}_{ijk}\}) \\ \mathcal{F}_1(Y, \hat{Y}) &= \frac{1}{N_c} \sum_{k=0}^2 \frac{2}{(C_{kk}/\sum_m C_{km}^T)^{-1} + (C_{kk}/\sum_m C_{km})^{-1}}\end{aligned}\tag{4.3}$$

In our latest work (in progress) in Figure 4.4, we used a more realistic propulsion system for 2 hours of real-time simulation, with an \mathcal{F}_1 score of 88%. A new mahalanobis distance method for unsupervised anomaly detection was developed to improve training labels.

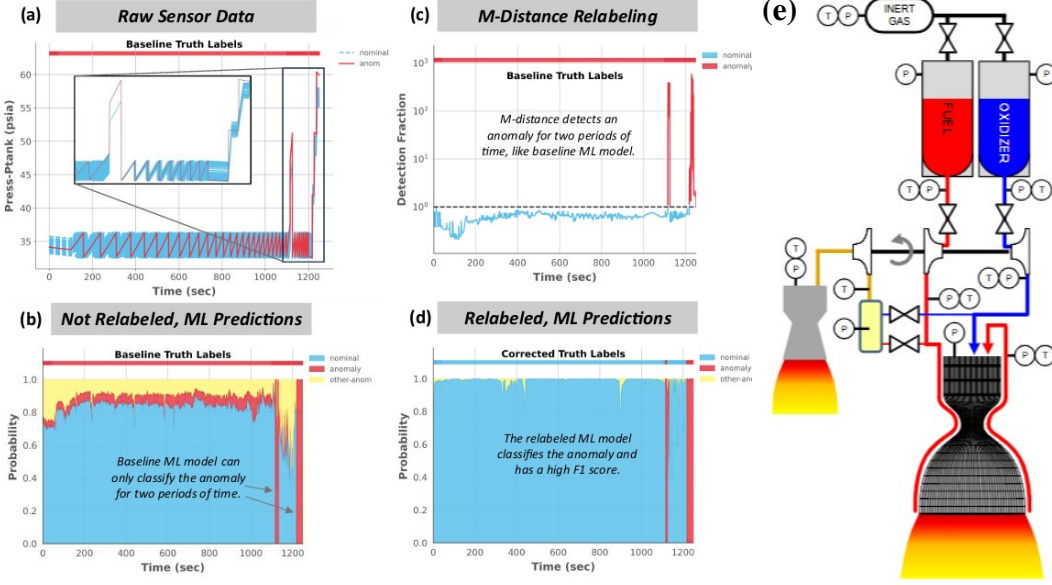


Figure 4.4: (a) Raw sensor data is fed into the ML model, with (c) the m-distance relabeling improving the \mathcal{F}_1 score by 18% from (b) the un-relabeled dataset to (d) the relabeled dataset. (e) A representative ground stage propulsion system from [114].

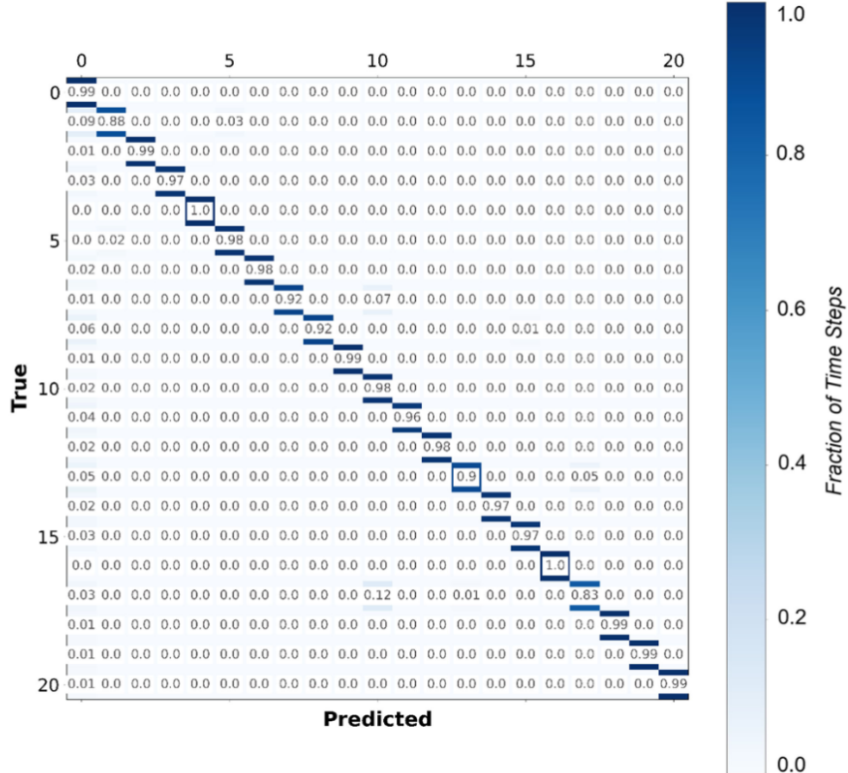


Figure 4.5: Confusion matrix across all timesteps of the time-series LSTM classifier in [J3]. A perfect model has ones on the diagonal indicating the truth and predictions match.

CHAPTER 5

HIGH-FIDELITY GEOMETRIC NONLINEAR AEROSTRUCTURAL OPTIMIZATION

The goal here is to speedup the high-fidelity analysis and optimization of geometric nonlinear, aerostructural design optimization problems with GPU computing, scalable linear solvers, and parametric ROMs I will use a GPU version of TACS, a GPU version of FUN3D, and FUNtoFEM and MELD for aerostructural coupling. For the ROMs in section 5.2, I will use a GPU version of our in-house CFD code and add a mesh deformation solver. The intended work of this section addresses the challenges for aerostructural design identified in section 3.2.

- *High computational cost of coupled analysis* - GPU computing, matrix-free linear solvers, and parametric ROMs will be used to speedup the coupled analyses.
- *Optimization* - use constraint aggregation and SNOPT optimizer [105]. Explore log-scaling to improve conditioning of the structural constraints and variables.
- *CFD mesh deformation* - use the inverse-distance weighted mesh deformation of Secco and Kenway [115], with GPUs and automatic differentiation. Secco and Kenway's mesh deformation makes up only 0.1% of the CFD runtime, whereas our current FUN3D and FUNtoFEM approach uses about 50% of the CFD runtime.

The novelty is a fully GPU aerostructural optimization tool for geometric nonlinear structures. Also, the use of GPUs in parametric ROMs of our tool will be explored.

5.1 Efficient High-Fidelity Analysis

TACS [70] was originally written for CPU parallelism. I've written a new C++ code `gpu_fem` which solves the director shell elements [116] from TACS on the GPU with

automatic differentiation. Next steps are improved linear solvers, put our in-house CFD code on the GPU, and build a GPU aerostructural coupling framework in FUNtoFEM and MELD. The following subsections detail the computational methods.

5.1.1 Automatic Differentiation

Hand-differentiation of high-fidelity analysis can become a time sink, so our team developed a code for nearly automatic differentiation (A2D) [117]. A2D is a C++ library with forward and reverse automatic differentiation (AD). The reverse AD of matrices and vectors comes from Giles [118], and is similar to backpropagation in machine learning [119].

Suppose we wish to compute derivatives of a functional $f \in \mathbb{R}$ for intermediate states, $x \in \mathbb{R}^n$, $y \in \mathbb{R}^m$, with gradients $\bar{x}_i = \frac{\partial f}{\partial x_i}$ and $\bar{y}_j = \frac{\partial f}{\partial y_j}$. Also define forward projection vectors \dot{x}_i , \dot{y}_j and projected Hessians $\hat{x}_i = \frac{\partial^2 f}{\partial x_i \partial x_j} \dot{x}_j$ and $\hat{y}_i = \frac{\partial^2 f}{\partial y_i \partial y_j} \dot{y}_j$. The gradients and projected Hessians in reverse AD are backpropagated through the chain rule below.

$$\begin{aligned} \text{(first order)} : \quad & \bar{x}_i = \bar{y}_j \cdot \frac{\partial y_j}{\partial x_i} \\ \text{(second order)} : \quad & \hat{x}_i = \hat{y}_k \cdot \frac{\partial y_k}{\partial x_i} + \bar{y}_k \frac{\partial^2 y_k}{\partial x_i \partial x_j} \dot{x}_j \end{aligned} \tag{5.1}$$

Reverse AD was implemented for the shell elements in `gpu_fem` on the steps from the displacement gradients $\frac{\partial u_i}{\partial x_j}$ to the strain energy U_e .

5.1.2 GPU Parallel Computing

Only recently have GPUs been available for general purpose programming [120]. Many high-fidelity analysis codes are switching from CPUs to heterogeneous CPU-GPU architectures to leverage the high parallel throughput of GPUs [121, 122, 123].

In our code `gpu_fem`, I've used GPU programming in CUDA [124] to assemble the residual $R(x, u)$ and jacobian matrix $K_t(x, u)$ for geometric nonlinear shells. The jacobian matrix $K_t(x, u)$ is assembled into a Block Sparse Row (BSR) format with the fill pattern

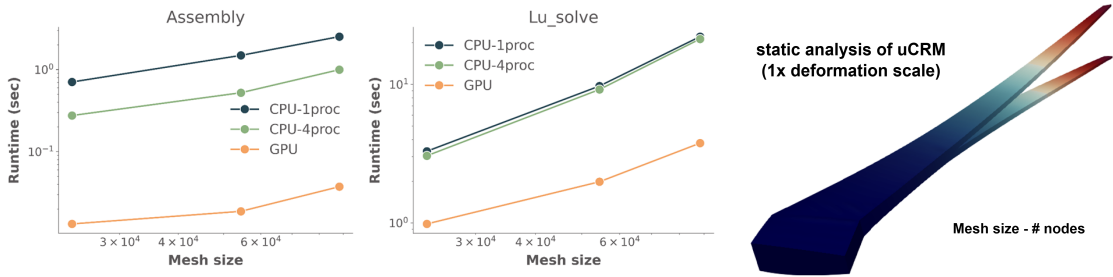


Figure 5.1: Jacobian assembly and cusparse direct LU solve on the GPU for the uCRM.

pre-computed on the host. The CUDA kernel computes one column of the element stiffness matrix $K_e(x_e, u_e)$ and one quadrature point per thread, which reduces the thread loading and increases performance. Figure 5.1 shows the GPU jacobian assembly and direct LU cusparse solve for the uCRM wing [125]. In this demo, the assembly has a 2x speedup and the LU solve with cusparse [126] has a 5.8x speedup compared to a 48 proc CPU estimate. Director shell elements require more memory per thread than other elements which can reduce parallelism, so additional tuning of the CUDA kernel may be needed.

5.1.3 Scalable Linear and Nonlinear Solvers

The three main costs of a high-fidelity analysis are (1) symbolic and numeric factorization of the sparse matrix, (2) assembly of the residual and jacobian, and (3) the linear solve. Linear systems are solved by direct methods - the LU and Cholesky, or iterative methods - GMRES, Preconditioned Conjugate Gradient, etc. [127]. Iterative methods tend to be faster for a single linear solve while direct methods tend to be faster for multiple right hand sides such as for an aerostructural problem with a linear structure. Also, direct methods perform better on the CPU and in CSR matrix format, while iterative methods such as GMRES perform better on the GPU, especially with matrix-vector products and BSR matrices.

Since we are doing geometric nonlinear aerostructural optimization, our jacobian matrix $K_t(x, u)$ is changing and iterative methods are preferred. For a fast nonlinear structures solve, we will do the following:

- Solve the linear system with the GMRES iterative solver on the GPU. Use matrix-free, matrix-vector products and a matrix-free ILU(k) preconditioner in cusparse.
- Stabilize the ILU(k) preconditioner with Reverse-Cuthill-Mcgee reordering [128] to reduce matrix bandwidth and the q-ordering step [129] to reduce chain lengths.
- Implement Newton’s method [2] and the Riks method [3] for nonlinear structures. The matrix Lagrange method will enforce the arc length constraint.
- Implement a continuation strategy [6] to restart the nonlinear solution during aerostructural optimization.

5.1.4 Aerostructural Coupling

We already have a framework for aeroelastic and aerothermoelastic analysis and optimization in FUNtoFEM in python on the CPU. I will be re-implementing FUNtoFEM and MELD into C++, with GPU or device pointers. Displacements will be transferred to a mesh deformation analysis and CFD solve in our in-house code Arrow, also on the GPU. I will implement the inverse distance weighted mesh deformation analysis of Secco [115] due to its efficiency, but may use GPUs to avoid kd-trees and speedup development time.

5.2 Parametric ROMs for Aerostructural Design

First ROMs for geometric nonlinear structural optimization will be built online with global POD and Qjan’s trust region method with error bounds [49, 130]. The global POD approach is preferred here over operator learning [45] as structural optimizations of stiffened structures contain on the order of thousands of design variables. Snapshots from the nonlinear structures solution $U = [u_1, \dots, u_n]$ will be used to construct a reduced basis $\Phi = [\phi_1, \dots, \phi_m]$ with m the number of modes selected by a singular value threshold. Once the reconstruction error is small enough, the optimization will solve the nonlinear structures problem with the reduced residual R_r^S (below) and reduced state $u_r \in \text{span}(\Phi)$.

$$R_r^S(x, u_r) = \Phi^T K_t(x, \Phi u_r) \Phi u_r - \Phi^T f \quad (5.2)$$

Hyper-reduction is a common strategy to reduce assembly time for the nonlinear residual R_r^S [50, 46] with QDEIM hyper-reduction the new state-of-the-art [51]. Nevertheless, with GPUs, the assembly of the reduced matrix $K_r(x, u_r) = \Phi^T K_t(x, \Phi u_r) \Phi$ can be achieved very cheaply using GPU parallelism. The steps are (1) compute the full state $u = \Phi u_r$, (2) compute m intermediate vectors $v_j = K_t(x, \Phi u_r) \phi_j$ using the assemble residual kernel, and (3) perform m^2 dot products $[K_r]_{ij} = \phi_i^T v_j$. Since assemble residual for shell elements parallelizes even better than the jacobian assembly on the GPU, the reduced matrix can be computed exceptionally cheaply and hyper-reduction may not be needed.

Then, aeroelastic ROMs using the aeroelastic high-fidelity analysis from section 5.1 will be built with separate POD reduced bases for the fluids and structures disciplines Φ^f, Φ^s . The structures discipline will still use global POD while the fluids discipline will use a combination of global POD and manifold interpolation [47]. As the global POD breaks down for fluids ROMs with changes in mach number and angle of attack [53], separate global PODs will be stored at different aerodynamic design points.

The following will be done to develop parametric ROMs for steady-state aerostructural optimization with aerodynamic, structural and shape variables.

- Compare the runtime of GPU assembly of the reduced matrix to hyper-reduction for geometric nonlinear ROMs - use the faster one for fluids ROMs as well.
- Develop ROMs for steady-state aerostructural optimization.
- Compare global POD, grassman manifold (differentiable) POD for fluid ROMs.
- Consider operator learning [55] or kernel POD for fluids ROMs, with fewer design variables due to a structural sizing ROM (section 2.3).
- Use trust region error bounds for online POD training [49].

CHAPTER 6

CONCLUSION

6.1 Remaining Publications

The aerostructural optimizations will all be steady-state in papers (3,4) . Also, publication (2) is nearly done and publication (1) will likely be fairly quick.

- 1) A publication exploring the use of **geometric programming** to speedup preliminary structural sizing and design optimizations for stiffened aircraft structures.
- 2) A second publication on *automated anomaly identification of launch vehicle propulsion systems*, with a longer 2 hour simulation time and my novel **mahanobis distance, statistics detection method** (nearly done, just writing).
- 3) A publication exploring the use of **GPU programming** and **scalable linear, nonlinear solvers** for high-fidelity geometric nonlinear aerostructural optimizations.
- 4) A publication using **parametric ROMs** to speedup high-fidelity, geometric nonlinear, aerostructural design optimization. (may be combined with previous)

6.2 Final Discussion

Briefly describe the timeline, my completed and remaining work. The novelties of my work here, what I hope to learn from this work.

REFERENCES

Journal Publications

- [J1] S. P. Engelstad, Z. M. Chen, and V. K. Goyal, “Analysis methodology for the assessment of unvented honeycomb sandwich structures subject to in-plane and pressure loads,” *Journal of Sandwich Structures & Materials*, vol. 25, no. 1, pp. 95–111, 2023. eprint: <https://doi.org/10.1177/10996362221122701>.
- [J2] S. P. Engelstad, B. J. Burke, and G. J. Kennedy, “Machine learning to improve buckling predictions for efficient structural optimization of stiffened structures,” in *AIAA Journal 2025*, To be submitted, 2025.
- [J3] S. P. Engelstad, S. R. Darr, T. A. Knighton, M. Taliaferro, V. K. Goyal, and G. J. Kennedy, “Machine-learning and physics-based tool for anomaly identification in propulsion systems,” *Journal of Spacecraft and Rockets*, vol. 61, no. 5, pp. 1219–1232, 2024. eprint: <https://doi.org/10.2514/1.A35897>.

Conference Papers

- [C1] B. J. Burke, S. P. Engelstad, and G. Kennedy, “Evaluation of open aeroelastic benchmark model for optimization in funtofem,” in *Proceedings of the AIAA SCITECH 2025 Forum*, 2025. eprint: <https://arc.aiaa.org/doi/pdf/10.2514/6.2025-2814>.
- [C2] S. P. Engelstad, Z. M. Chen, V. K. Goyal, and S. Maghsoudy-Louyeh, “Design curves for unvented honeycomb sandwich structures subject to in-plane and pressure loads,” in *AIAA SCITECH 2022 Forum*, 2022. eprint: <https://arc.aiaa.org/doi/pdf/10.2514/6.2022-0668>.
- [C3] S. P. Engelstad, B. J. Burke, and G. J. Kennedy, “Machine learning to improve buckling predictions for efficient structural optimization of aircraft wings,” in *AIAA AVIATION FORUM AND ASCEND 2024*, 2024. eprint: <https://arc.aiaa.org/doi/pdf/10.2514/6.2024-3981>.
- [C4] S. P. Engelstad, B. J. Burke, R. N. Patel, S. Sahu, and G. J. Kennedy, “High-fidelity aerothermoelastic optimization with differentiable cad geometry,” in *Proceedings of the AIAA SCITECH 2023 Forum*. eprint: <https://arc.aiaa.org/doi/pdf/10.2514/6.2023-0329>.
- [C5] S. P. Engelstad, E. Zeitunian, V. K. Goyal, B. J. Burke, and G. Kennedy, “Stability analysis considerations for geometrically imperfect cylinders under thermomechanical loads,” in *AIAA SCITECH 2025 Forum*, 2025. eprint: <https://arc.aiaa.org/doi/pdf/10.2514/6.2025-0441>.
- [C6] S. R. Darr, S. Engelstad, T. Knighton, M. E. Taliaferro, and V. K. Goyal, “A combined machine learning and physics-based tool for anomaly identification in propulsion systems,” in *AIAA SCITECH 2023 Forum*. eprint: <https://arc.aiaa.org/doi/pdf/10.2514/6.2023-2375>.

Other References

- [1] M. Castellani, J. E. Cooper, and Y. Lemmens, “Nonlinear static aeroelasticity of high-aspect-ratio-wing aircraft by finite element and multibody methods,” *Journal of Aircraft*, vol. 54, no. 2, pp. 548–560, 2017.
- [2] J. N. Reddy, *An Introduction to Nonlinear Finite Element Analysis*, 2nd. Oxford University Press, 2015.
- [3] E. Riks, “An incremental approach to the solution of snapping and buckling problems,” *International Journal of Solids and Structures*, vol. 15, no. 7, pp. 529–551, 1979.
- [4] W. Su and C. E. S. Cesnik, “Nonlinear aeroelasticity of a very flexible blended-wing-body aircraft,” *Journal of Aircraft*, vol. 47, no. 5, pp. 1539–1553, 2010. eprint: <https://doi.org/10.2514/1.47317>.
- [5] M. Patil and D. Hodges, “On the importance of aerodynamic and structural geometrical nonlinearities in aeroelastic behavior of high-aspect-ratio wings,” *Journal of Fluids and Structures*, vol. 19, no. 7, pp. 905–915, 2004.
- [6] R. Sanchez, T. Albring, R. Palacios, N. R. Gauger, T. D. Economon, and J. J. Alonso, “Coupled adjoint-based sensitivities in large-displacement fluid-structure interaction using algorithmic differentiation,” *International Journal for Numerical Methods in Engineering*, vol. 113, no. 7, pp. 1081–1107, 2018. eprint: <https://onlinelibrary.wiley.com/doi/pdf/10.1002/nme.5700>.
- [7] A. C. Gray and J. R. Martins, “Geometrically nonlinear high-fidelity aerostructural optimization for highly flexible wings,” in *AIAA Scitech 2021 Forum*. eprint: <https://arc.aiaa.org/doi/pdf/10.2514/6.2021-0283>.
- [8] J. J. McNamara and P. P. Friedmann, “Aeroelastic and aerothermoelastic analysis in hypersonic flow: Past, present, and future,” *AIAA Journal*, vol. 49, no. 6, pp. 1089–1122, 2011. eprint: <https://doi.org/10.2514/1.J050882>.
- [9] A. J. Culler and J. J. McNamara, “Studies on fluid-thermal-structural coupling for aerothermoelasticity in hypersonic flow,” *AIAA Journal*, vol. 48, no. 8, pp. 1721–1738, 2010. eprint: <https://doi.org/10.2514/1.J050193>.
- [10] P. Friedmann, B. Thuruthimattam, J. McNamara, and K. Powell, “Hypersonic aeroelasticity and aerothermoelasticity with application to reusable launch vehicles,” in *Proceedings of the 12th AIAA International Space Planes and Hypersonic Systems and Technologies*, 2003. eprint: <https://arc.aiaa.org/doi/pdf/10.2514/6.2003-7014>.
- [11] M. A. Akgun, R. T. Haftka, K. C. Wu, J. L. Walsh, and J. H. Garcelon, “Efficient structural optimization for multiple load cases using adjoint sensitivities,” *AIAA Journal*, vol. 39, no. 3, pp. 511–516, 2001. eprint: <https://doi.org/10.2514/2.1336>.
- [12] J. R. R. A. Martins, P. Sturdza, and J. J. Alonso, “The complex-step derivative approximation,” *ACM Trans. Math. Softw.*, vol. 29, no. 3, pp. 245–262, Sep. 2003.
- [13] G. J. Kennedy and J. R. R. A. Martins, “A parallel aerostructural optimization framework for aircraft design studies,” *Structural and Multidisciplinary Optimization*, vol. 50, no. 6, pp. 1079–1101, 2014.

- [14] A. C. Gray and J. R. Martins, “A proposed benchmark model for practical aeroelastic optimization of aircraft wings,” in *AIAA SCITECH 2024 Forum*, 2024. eprint: <https://arc.aiaa.org/doi/pdf/10.2514/6.2024-2775>.
- [15] G. J. Kennedy, “Strategies for adaptive optimization with aggregation constraints using interior-point methods,” *Computers Structures*, vol. 153, pp. 217–229, 2015.
- [16] A. B. Lambe, J. R. R. A. Martins, and G. J. Kennedy, “An evaluation of constraint aggregation strategies for wing box mass minimization,” *Structural and Multidisciplinary Optimization*, vol. 55, no. 1, pp. 257–277, 2017.
- [17] A. B. Lambe and J. R. R. A. Martins, “Matrix-free aerostructural optimization of aircraft wings,” *Structural and Multidisciplinary Optimization*, vol. 53, no. 3, pp. 589–603, 2016.
- [18] S. Arreckx, A. B. Lambe, J. R. R. A. Martins, and D. Orban, “A matrix-free augmented lagrangian algorithm with application to large-scale structural design optimization,” *Optimization and Engineering*, vol. 17, no. 2, pp. 359–384, Jun. 2016.
- [19] A. B. Lambe, “A matrix-free algorithm for multidisciplinary design optimization,” Ph.D. dissertation, University of Toronto, 2012.
- [20] M. Avriel, *Advances in Geometric Programming* (Mathematical Concepts and Methods in Science and Engineering). Springer US, 1980, vol. 21.
- [21] M. Avriel, R. Dembo, and U. Passy, “Solution of generalized geometric programs,” *International Journal for Numerical Methods in Engineering*, vol. 9, no. 1, pp. 149–168, 1975. eprint: <https://onlinelibrary.wiley.com/doi/pdf/10.1002/nme.1620090112>.
- [22] S. Boyd and L. Vandenberghe, *Convex Optimization*. Cambridge University Press, 2004.
- [23] S. Boyd, S.-J. Kim, L. Vandenberghe, and A. Hassibi, “A tutorial on geometric programming,” Stanford University, Tech. Rep., 2007.
- [24] W. Hoburg and P. Abbeel, “Geometric programming for aircraft design optimization,” *arXiv preprint arXiv:1210.6980*, 2014.
- [25] W. Hoburg, “Aircraft design optimization as a geometric program,” PhD Thesis, University of California, Berkeley, 2015.
- [26] T.-Y. Chen, “Structural optimization using single-term posynomial geometric programming,” *Computers Structures*, vol. 45, no. 5, pp. 911–918, 1992.
- [27] A. Chan and E. Turlea, “An approximate method for structural optimisation,” *Computers Structures*, vol. 8, no. 3, pp. 357–363, 1978.
- [28] P. Hajela, “Geometric programming strategies in large-scale structural synthesis,” *AIAA Journal*, vol. 24, no. 7, pp. 1173–1178, 1986. eprint: <https://doi.org/10.2514/3.9410>.
- [29] N. Ali, K. Behdinan, and Z. Fawaz, “Applicability and viability of a ga based finite element analysis architecture for structural design optimization,” *Computers Structures*, vol. 81, no. 22, pp. 2259–2271, 2003.
- [30] G. Rozvany, *Structural Design via Optimality Criteria: The Prager Approach to Structural Optimization*. Dordrecht: Springer, 1989, ISBN: 978-94-009-1161-1.
- [31] J. Kiusalaas, “Minimum Weight Design of Structures via Optimality Criteria,” NASA Marshall Space Flight Center, Tech. Rep. NASA-TN-D-7115, Dec. 1972.

- [32] J. Kiusalaas and G. B. Reddy, “DESAP 2: A Structural Design Program with Stress and Buckling Constraints. Volume 1: Theoretical and User’s Manual,” NASA Ames Research Center, Tech. Rep. NASA CR-2797, Mar. 1977.
- [33] P. K. Gotsis, “Structural optimization of thin shells using finite element method,” NASA Lewis Research Center, Cleveland, Ohio, Tech. Rep. TM-105903, 1992.
- [34] G. J. Kennedy, G. K. W. Kenway, and J. R. R. Martins, “A comparison of metallic, composite and nanocomposite optimal transonic transport wings,” NASA Technical Reports Server (NTRS), Tech. Rep. NASA/CR-2014-218185, 2014.
- [35] A. B. Rashid and M. A. K. Kausik, “Ai revolutionizing industries worldwide: A comprehensive overview of its diverse applications,” *Hybrid Advances*, vol. 7, p. 100277, 2024.
- [36] S. Le Clainche, E. Ferrer, S. Gibson, E. Cross, A. Parente, and R. Vinuesa, “Improving aircraft performance using machine learning: A review,” *arXiv preprint arXiv:2210.11481*, 2022.
- [37] C. E. Rasmussen and C. K. I. Williams, *Gaussian Processes for Machine Learning*. The MIT Press, 2006.
- [38] S. Hochreiter and J. Schmidhuber, “Long short-term memory,” *Neural Computation*, vol. 9, no. 8, pp. 1735–1780, Nov. 1997. eprint: <https://direct.mit.edu/neco/article-pdf/9/8/1735/813796/neco.1997.9.8.1735.pdf>.
- [39] A. S. Thelen, D. E. Bryson, B. K. Stanford, and P. S. Beran, “Multi-fidelity gradient-based optimization for high-dimensional aeroelastic configurations,” *Algorithms*, vol. 15, no. 4, 2022.
- [40] N. Wu, C. A. Mader, and J. R. R. Martins, “Large-scale multifidelity aerostructural optimization of a transport aircraft,” in *33rd Congress of the International Council of the Aeronautical Sciences*, Stockholm, Sweden, Sep. 2022.
- [41] A. Crovato, A. P. Prado, P. H. Cabral, R. Boman, V. E. Terrapon, and G. Dimitriadis, “A discrete adjoint full potential formulation for fast aerostructural optimization in preliminary aircraft design,” *Aerospace Science and Technology*, vol. 138, p. 108332, 2023.
- [42] J. N. Kutz, S. L. Brunton, B. W. Brunton, and J. L. Proctor, *Dynamic Mode Decomposition: Data-Driven Modeling of Complex Systems* (Advances in Design and Control). SIAM, 2016.
- [43] M. O. Williams, C. W. Rowley, and I. G. Kevrekidis, “A kernel-based method for data-driven koopman spectral analysis,” *arXiv preprint arXiv:1411.2260*, 2014.
- [44] P. J. Baddoo, B. Herrmann, B. J. McKeon, and S. L. Brunton, “Kernel learning for robust dynamic mode decomposition: Linear and nonlinear disambiguation optimization (lando),” *arXiv preprint arXiv:2106.01510*, 2021.
- [45] P. Benner, S. Gugercin, and K. Willcox, “A survey of projection-based model reduction methods for parametric dynamical systems,” *SIAM Review*, vol. 57, no. 4, pp. 483–531, 2015.
- [46] D. Amsallem, M. Zahr, Y. Choi, and C. Farhat, “Design optimization using hyper-reduced-order models,” *Structural and Multidisciplinary Optimization*, vol. 51, no. 4, pp. 919–940, 2015.

- [47] D. Amsallem and C. Farhat, “Interpolation method for adapting reduced-order models and application to aeroelasticity,” *AIAA Journal*, vol. 46, no. 7, pp. 1803–1813, 2008. eprint: <https://doi.org/10.2514/1.35374>.
- [48] S. A. McQuarrie, P. Khodabakhshi, and K. E. Willcox, “Nonintrusive reduced-order models for parametric partial differential equations via data-driven operator inference,” *SIAM Journal on Scientific Computing*, vol. 45, no. 4, A1917–A1946, 2023. eprint: <https://doi.org/10.1137/21M1452810>.
- [49] E. Qian, M. Grepl, K. Veroy, and K. Willcox, “A certified trust region reduced basis approach to pde-constrained optimization,” *SIAM Journal on Scientific Computing*, vol. 39, no. 5, S434–S460, 2017.
- [50] S. Chaturantabut and D. C. Sorensen, “Nonlinear model reduction via discrete empirical interpolation,” *SIAM Journal on Scientific Computing*, vol. 32, no. 5, pp. 2737–2764, 2010. eprint: <https://doi.org/10.1137/090766498>.
- [51] Z. Drmač and S. Gugercin, “A new selection operator for the discrete empirical interpolation method – improved a priori error bound and extensions,” *SIAM Journal on Scientific Computing*, vol. 38, no. 2, A631–A648, 2016.
- [52] T. Lieu, “An efficient approach to reduced-order modeling for nonlinear dynamic systems,” Ph.D. dissertation, University of California, Berkeley, 2004.
- [53] T. Lieu, C. Farhat, and M. Lesoinne, “Reduced-order fluid/structure modeling of a complete aircraft configuration,” *Computer Methods in Applied Mechanics and Engineering*, vol. 195, no. 41, pp. 5730–5742, 2006, John H. Argyris Memorial Issue. Part II.
- [54] G. Berkooz, P. Holmes, and J. L. Lumley, “The proper orthogonal decomposition in the analysis of turbulent flows,” *Annual Review of Fluid Mechanics*, vol. 25, no. Volume 25, 1993, pp. 539–575, 1993.
- [55] B. G. Zastrow, A. Chaudhuri, K. E. Willcox, A. S. Ashley, and M. C. Henson, “Data-driven model reduction via operator inference for coupled aeroelastic flutter,” in *Proceedings of the AIAA SciTech Forum*, 2023.
- [56] P. Hu, K. Ni, K. Qu, L. Xue, and H. Zhao, “An efficient pod/rom based aeroelasticity model,” Apr. 2010, ISBN: 978-1-60086-961-7.
- [57] B. Schölkopf, A. J. Smola, and K.-R. Müller, “Nonlinear component analysis as a kernel eigenvalue problem,” *Neural Computation*, vol. 10, no. 5, pp. 1299–1319, 1998.
- [58] P. Díez, A. Muixí, S. Zlotnik, and A. García-González, *Nonlinear dimensionality reduction for parametric problems: A kernel proper orthogonal decomposition (kpod)*, 2021. arXiv: 2104.13765 [math.NA].
- [59] D. Huang and P. P. Friedmann, “An aerothermoelastic analysis framework with reduced-order modeling applied to composite panels in hypersonic flows,” *Journal of Fluids and Structures*, vol. 94, p. 102 927, 2020.
- [60] D. Huang, P. P. Friedmann, and T. Rokita, “Aerothermoelastic scaling laws for hypersonic skin panel configurations with arbitrary flow orientation,” *AIAA Journal*, vol. 57, no. 10, pp. 4377–4392, 2019. eprint: <https://doi.org/10.2514/1.J057499>.

- [61] B. Mufti, C. Perron, and D. N. Mavris, “Multifidelity methodology for reduced-order models with high-dimensional inputs,” *AIAA Journal*, vol. 62, no. 10, pp. 3932–3947, 2024. eprint: <https://doi.org/10.2514/1.J064110>.
- [62] S. P. Timoshenko and S. Woinowsky-Krieger, *Theory of Plates and Shells*, 2nd. McGraw-Hill, 1959, ISBN: 978-0070858200.
- [63] V. Goyal, J. P. Tuck-Lee, J. Rome, *et al.*, “Failure analysis of unvented honeycomb structures,” in *29th ASC Technical Conference*, University of California at San Diego, La Jolla, CA, 2014.
- [64] M. Smith, *ABAQUS/Standard User’s Manual, Version 6.9*. United States: Dassault Systèmes Simulia Corp, 2009.
- [65] N. G. Tsouvalis and V. J. Papazoglou, “Design buckling curves for clamped orthotropic laminated plates,” *Advanced Composites Letters*, vol. 13, no. 5, 2004. eprint: <https://doi.org/10.1177/096369350401300502>.
- [66] E. J. Brunelle and G. A. Oyibo, “Generic buckling curves for specially orthotropic rectangular plates,” *AIAA Journal*, vol. 21, no. 8, pp. 1150–1156, 1983. eprint: <https://doi.org/10.2514/3.8219>.
- [67] C. Mittelstedt, “Closed-form buckling analysis of stiffened composite plates and identification of minimum stiffener requirements,” *International Journal of Engineering Science - INT J ENG SCI*, vol. 46, pp. 1011–1034, Oct. 2008.
- [68] S. Hosseini-Hashemi, S. R. Atashipour, and M. Fadaee, “On the buckling analysis of isotropic, transversely isotropic, and laminated rectangular plates via reddy plate theory: An exact closed-form procedure,” *Proceedings of the Institution of Mechanical Engineers, Part C: Journal of Mechanical Engineering Science*, vol. 226, no. 5, pp. 1210–1224, 2012. eprint: <https://doi.org/10.1177/0954406211422661>.
- [69] E. Ruocco and J. Reddy, “A closed-form solution for buckling analysis of orthotropic reddy plates and prismatic plate structures,” *Composites Part B: Engineering*, vol. 169, pp. 258–273, 2019.
- [70] G. J. Kennedy and J. R. R. A. Martins, “A parallel finite-element framework for large-scale gradient-based design optimization of high-performance structures,” *Finite Elements in Analysis and Design*, vol. 87, pp. 56–73, Sep. 2014.
- [71] T. R. Brooks, J. R. R. A. Martins, and G. J. Kennedy, “High-fidelity aerostructural optimization of tow-steered composite wings,” *Journal of Fluids and Structures*, vol. 88, pp. 122–147, Jul. 2019.
- [72] G. Kennedy, “A full-space barrier method for stress-constrained discrete material design optimization,” *Structural and Multidisciplinary Optimization*, vol. 54, Sep. 2016.
- [73] G. J. Kennedy and J. E. Hicken, “Improved constraint-aggregation methods,” *Computer Methods in Applied Mechanics and Engineering*, vol. 289, pp. 332–354, 2015.
- [74] J. Kiusalaas and G. B. Reddy, “DESAP I - A Structural Design Program with Stress and Displacement Constraints. Volume I: Theoretical and User’s Manual,” NASA Ames Research Center, Tech. Rep. NASA CR-2794, Feb. 1977.

- [75] G. Rozvany, “Stress ratio and compliance-based methods in topology optimization—a critical review,” *Structural and Multidisciplinary Optimization*, vol. 21, no. 2, pp. 109–119, 2001.
- [76] O. M. Querin, “Evolutionary structural optimisation: Stress based formulation and implementation,” Ph.D. Thesis, Ph.D. dissertation, Department of Aeronautical Engineering, University of Sydney, 1997.
- [77] M. Avriel, Ed., *Advances in Geometric Programming*. Springer US, 1980.
- [78] J. G. Ecker, “Geometric programming,” in *Encyclopedia of Operations Research and Management Science*, S. I. Gass and C. M. Harris, Eds. New York, NY: Springer US, 2001, pp. 330–332, ISBN: 978-1-4020-0611-1.
- [79] A. W. Max, “Inverting modified matrices,” in *Memorandum Rept. 42, Statistical Research Group*, Princeton Univ., 1950, p. 4.
- [80] S. Boyd, *A tutorial on convex optimization*, Accessed: 2025-02-21, 2018.
- [81] M. Patil and D. Hodges, “On the importance of aerodynamic and structural geometrical nonlinearities in aeroelastic behavior of high-aspect-ratio wings,” *Journal of Fluids and Structures*, vol. 19, no. 7, pp. 905–915, 2004.
- [82] T. VON KARMAN and H.-S. TSIEN, “The buckling of thin cylindrical shells under axial compression,” *Journal of the Aeronautical Sciences*, vol. 8, no. 8, pp. 303–312, 1941. eprint: <https://doi.org/10.2514/8.10722>.
- [83] W. T. Koiter, “The stability of elastic equilibrium,” 1970.
- [84] L. H. Donnell and C. C. Wan, “Effect of imperfections on buckling of thin cylinders and columns under axial compression,” *Journal of Applied Mechanics*, vol. 17, no. 1, pp. 73–83, Apr. 2021. eprint: https://asmedigitalcollection.asme.org/appliedmechanics/article-pdf/17/1/73/6746531/73_1.pdf.
- [85] M. W. Hilburger, “Buckling of thin-walled circular cylinders,” NASA Langley Research Center, Tech. Rep. NASA/SP-8007-2020/REV 2, 2020.
- [86] M. Mikulas, M. Nemeth, L. Oremont, and D. Jegley, “Effect of boundary conditions on the axial compression buckling of homogeneous orthotropic composite cylinders in the long column range,” in *52nd AIAA/ASME/ASCE/AHS/ASC Structures, Structural Dynamics and Materials Conference*. eprint: <https://arc.aiaa.org/doi/pdf/10.2514/6.2011-2126>.
- [87] L. H. Donnell, “A new theory for the buckling of thin cylinders under axial compression and bending,” *Transactions of the American Society of Mechanical Engineers*, vol. 56, no. 8, pp. 795–806, Feb. 2023. eprint: https://asmedigitalcollection.asme.org/fluidsengineering/article-pdf/56/8/795/6983686/795_1.pdf.
- [88] K. Jacobson, J. Kiviah, M. Smith, and G. Kennedy, “An aeroelastic coupling framework for time-accurate analysis and optimization,” in *2018 AIAA/ASCE/AHS/ASC Structures, Structural Dynamics, and Materials Conference*, Jan. 2018. eprint: <https://arc.aiaa.org/doi/pdf/10.2514/6.2018-0100>.
- [89] K. E. Jacobson, J. F. Kiviah, G. J. Kennedy, and M. J. Smith, “Evaluation of time-domain damping identification methods for flutter-constrained optimization,” *Journal of Fluids and Structures*, vol. 87, pp. 174–188, 2019.

- [90] K. E. Jacobson, “Adjoint-based aeroelastic optimization with high-fidelity time-accurate sensitivities,” Ph.D. dissertation, Georgia Institute of Technology, 2018.
- [91] L. Smith, L. Halim, G. Kennedy, and M. Smith, “A high-fidelity coupling framework for aerothermoelastic analysis and adjoint-based gradient evaluation,” in *AIAA Scitech 2021 Forum*, 2021. eprint: <https://arc.aiaa.org/doi/pdf/10.2514/6.2021-0407>.
- [92] L. J. Halim, S. Sahu, G. Kennedy, and M. Smith, “Aerothermoelastic analysis and optimization of stiffened thin-walled structures,” in *AIAA Scitech 2022 Forum*, 2022. eprint: <https://arc.aiaa.org/doi/pdf/10.2514/6.2022-1612>.
- [93] R. Haimes and J. Dannenhoffer, “The engineering sketch pad: A solid-modeling, feature-based, web-enabled system for building parametric geometry,” in *21st AIAA Computational Fluid Dynamics Conference*, 2013.
- [94] J. Dannenhoffer, “Opencsm: An open-source constructive solid modeler for mdao,” in *21st AIAA Fluid Dynamic Conference*, 2013.
- [95] N. Novotny, D. Sandler, and N. A. Wukie, “Gradient-based aeroelastic optimization of a generic flying wing model,” in *AIAA SCITECH 2025 Forum*, 2025. eprint: <https://arc.aiaa.org/doi/pdf/10.2514/6.2025-1749>.
- [96] N. L. Novotny, “An exergy approach for high-fidelity analysis and optimization of aerospace systems,” Ph.D. dissertation, University of Dayton, 2024.
- [97] R. T. Biedron, J.-R. Carlson, J. M. Derlaga, *et al.*, “Fun3d manual: 13.6,” National Aeronautics and Space Administration, Langley Research Center, Hampton, VA, Tech. Rep. 2019-220416, Oct. 2019.
- [98] K. W. Anderson, J. C. Newman, and S. L. Karman, “Stabilized finite elements in fun3d,” *Journal of Aircraft*, vol. 55, no. 2, Mar. 2018.
- [99] E. J. Nielsen, J. Lu, M. A. Park, and D. L. Darmofal, “An implicit, exact dual adjoint solution method for turbulent flows on unstructured grids,” *Computers & Fluids*, vol. 33, no. 9, pp. 1131–1155, Nov. 2004.
- [100] R. T. Biedron and J. L. Thomas, “Recent enhancements to the fun3d flow solver for moving-mesh applications,” *AIAA 2009-1360*, no. 1360, 2009.
- [101] J. Dannenhoffer and R. Haimes, “Generation of multi-fidelity, multi-discipline air vehicle models with the engineering sketch pad,” no. 1925, 2016.
- [102] J. Dannenhoffer and R. Haimes, “Design sensitivity calculations directly on cad-based geometry,” in *2015 AIAA Scitech Forum*, 2015.
- [103] J. Kiviah and G. Kennedy, “Efficient and robust load and displacement transfer scheme using weighted least squares,” *AIAA Journal*, vol. 57, no. 5, pp. 2237–2243, 2019.
- [104] B. M. Irons and R. C. Tuck, “A version of the Aitken accelerator for computer iteration,” *International Journal for Numerical Methods in Engineering*, vol. 1, no. 3, pp. 275–277, 1969.
- [105] E. Wu, G. Kenway, C. A. Mader, J. Jasa, and J. R. R. A. Martins, “Pyoptsparse: A python framework for large-scale constrained nonlinear optimization of sparse systems,” *Journal of Open Source Software*, vol. 5, no. 54, p. 2564, 2020.

- [106] F. M. A. Mitrotta, A. Pirrera, and J. E. Cooper, “Preliminary aeroelastic optimization of the simple transonic wing with nonlinear structural stability constraints,” in *AIAA SCITECH 2025 Forum*, 2025. eprint: <https://arc.aiaa.org/doi/pdf/10.2514/6.2025-2811>.
- [107] S. Guarro, “Launch vehicle reliability and risk metrics definition and estimation in relation to requirements,” in *Probabilistic Safety Assessment and Management PSAM 14*, 2018.
- [108] C. H. Williams, L. J. Ross, and J. J. Nieberding, “A prognostic launch vehicle probability of failure assessment methodology for conceptual systems predicated on human causal factors,” in *2018 AIAA SPACE and Astronautics Forum and Exposition*, 2018. eprint: <https://arc.aiaa.org/doi/pdf/10.2514/6.2018-5413>.
- [109] J. M. Rising and N. G. Leveson, “Systems-theoretic process analysis of space launch vehicles,” *Journal of Space Safety Engineering*, vol. 5, no. 3, pp. 153–183, 2018.
- [110] F. A. Gers, J. Schmidhuber, and F. Cummins, “Learning to forget: Continual prediction with lstm,” *Neural Computation*, vol. 12, no. 10, pp. 2451–2471, Oct. 2000. eprint: <https://direct.mit.edu/neco/article-pdf/12/10/2451/814643/089976600300015015.pdf>.
- [111] M. E. Taliaferro and S. R. Darr, “Modeling internal launch vehicle fluid flow and thermodynamics, part 1: Thermodynamic tank network solver,” in *AIAA SCITECH 2024 Forum*, 2024. eprint: <https://arc.aiaa.org/doi/pdf/10.2514/6.2024-2293>.
- [112] Martín Abadi *et al.*, *TensorFlow: Large-scale machine learning on heterogeneous systems*, Software available from tensorflow.org, 2015.
- [113] J. Opitz and S. Burst, “Macro f1 and macro f1,” *arXiv preprint*, 2019. arXiv: 1911.03347 [cs.LG].
- [114] V. K. Goyal *et al.*, “Applications of machine learning to launch vehicles,” in *AIAA SCITECH 2024 Forum*, 2024. eprint: <https://arc.aiaa.org/doi/pdf/10.2514/6.2024-1209>.
- [115] N. R. Secco, G. K. W. Kenway, P. He, C. Mader, and J. R. R. A. Martins, “Efficient mesh generation and deformation for aerodynamic shape optimization,” *AIAA Journal*, vol. 59, no. 4, pp. 1151–1168, 2021. eprint: <https://doi.org/10.2514/1.J059491>.
- [116] J. Simo and D. Fox, “On a stress resultant geometrically exact shell model. part i: Formulation and optimal parametrization,” *Computer Methods in Applied Mechanics and Engineering*, vol. 72, no. 3, pp. 267–304, 1989.
- [117] Y. Fu, B. Li, and G. J. Kennedy, “Multiphysics simulation and optimization using high-order finite elements with structured differentiation,” in *AIAA SCITECH 2023 Forum*, 2023. eprint: <https://arc.aiaa.org/doi/pdf/10.2514/6.2023-0530>.
- [118] M. B. Giles, “Collected matrix derivative results for forward and reverse mode algorithmic differentiation,” in *Advances in Automatic Differentiation*, C. H. Bischof, H. M. Bücker, P. Hovland, U. Naumann, and J. Utke, Eds., Berlin, Heidelberg: Springer Berlin Heidelberg, 2008, pp. 35–44, ISBN: 978-3-540-68942-3.
- [119] A. G. Baydin, B. A. Pearlmutter, A. A. Radul, and J. M. Siskind, “Automatic differentiation in machine learning: A survey,” *Journal of Machine Learning Research*, vol. 18, no. 153, pp. 1–43, 2018.
- [120] J. Cheng, M. Grossman, and T. McKercher, *Professional CUDA C Programming*. Indianapolis, IN: Wiley, 2014, ISBN: 978-1-118-73932-7.

- [121] P. Fischer *et al.*, “Scalability of high-performance pde solvers,” *The International Journal of High Performance Computing Applications*, vol. 34, no. 5, pp. 562–586, 2020. eprint: <https://doi.org/10.1177/1094342020915762>.
- [122] J. Brown *et al.*, “Performance portable solid mechanics via matrix-free \$p\$-multigrid,” *arXiv preprint arXiv:2204.01722*, 2022.
- [123] A. Abdelfattah *et al.*, “Gpu algorithms for efficient exascale discretizations,” *Parallel Computing*, vol. 108, p. 102 841, 2021.
- [124] NVIDIA, P. Vingelmann, and F. H. Fitzek, *Cuda, release: 10.2.89*, 2020.
- [125] T. R. Brooks, G. K. Kenway, and J. R. R. A. Martins, “Undeflected common research model (ucrm): An aerostructural model for the study of high aspect ratio transport aircraft wings,” in *35th AIAA Applied Aerodynamics Conference*. eprint: <https://arc.aiaa.org/doi/pdf/10.2514/6.2017-4456>.
- [126] X. Zhang, H. Liu, and Y. Li, *Pellr: A permuted ellpack-r format for spmv on gpus*, Accessed: 2025-02-17, 2025.
- [127] Y. Saad, *Iterative Methods for Sparse Linear Systems*, 2nd. Society for Industrial and Applied Mathematics, 2003.
- [128] E. Cuthill and J. McKee, “Reducing the bandwidth of sparse symmetric matrices,” in *Proceedings of the 1969 24th National Conference*, ser. ACM ’69, New York, NY, USA: Association for Computing Machinery, 1969, pp. 157–172, ISBN: 9781450374934.
- [129] W. K. Anderson, S. Wood, and K. E. Jacobson, “Node numbering for stabilizing preconditioners based on incomplete lu decomposition,” in *AIAA AVIATION 2020 FORUM*, 2020. eprint: <https://arc.aiaa.org/doi/pdf/10.2514/6.2020-3022>.
- [130] Y. Yue and K. Meerbergen, “Accelerating optimization of parametric linear systems by model order reduction,” *SIAM Journal on Optimization*, vol. 23, no. 2, pp. 1344–1370, 2013. eprint: <https://doi.org/10.1137/120869171>.